Neutron emission as a probe of fusion-fission and quasifission dynamics

D. J. Hinde
Hahn-Meitner-Institut Berlin, D-1000 Berlin 39, Germany
and Department of Nuclear Physics, Research School of Physical Sciences and Engineering, Australian National University, GPO Box 4, Canberra, ACT 2601, Australia

D. Hilscher, H. Rossner, B. Gebauer, M. Lehmann, and M. Wilpert
Hahn-Meitner-Institut Berlin, D-1000 Berlin 39, Germany
(Received 6 September 1991)

Pre-scission and post-scission neutron yields have been measured as a function of projectile mass, compound nucleus fissility, and fission mass split and total kinetic energy (TKE) for 27 fusion-fission and quasifission reactions induced by beams of ^{16,18}O, ^{40}Ar, and ^{64}Ni. A new method of interpretation of experimental pre-scission neutron multiplicities ν_{pre} and mean kinetic energies ε_ν allows the extraction of fission time scales with much less uncertainty than previously, all fusion-fission results being consistent with a dynamical time scale of $(35\pm15)\times10^{-21}$ s for symmetric fission. All reactions show that ν_{pre} falls quite rapidly with increasing mass asymmetry; evidence is presented that for fusion-fission reactions this is partly due to a reduction of the dynamical fission time scale with mass asymmetry. For quasifission, the data indicate that the pre-scission multiplicity and mean neutron kinetic energy are very sensitive to the final mass asymmetry, but that the time scale is virtually independent of mass asymmetry. It is concluded that for fusion-fission there is no dependence of ν_{pre} on TKE, while for ^{64}Ni-induced quasifission reactions, a strong increase of ν_{pre} with decreasing TKE is observed. This is probably largely caused by neutron emission during the acceleration time of the fission fragments in these fast reactions. Interpretation of post-scission multiplicities in terms of fragment excitation energies leads to deduced time scales consistent with those determined from the pre-scission data.

PACS number(s): 25.70.Jj, 25.85.Ge

I. INTRODUCTION

The confrontation between experimental data and theoretical pictures of the dynamics of fission and quasifission has largely been in the areas of the average total kinetic energy [1,2] (TKE) and its width [3,4], the width of fission mass distributions [5-9], and angular distributions of the massive partners in the binary fragmentation [7,10–13]. Very valuable insights into these processes have been obtained from such work. In the last decade, a rapidly increasing body of experimental data on the properties of the light particles emitted during such heavy-ion-induced reactions has been obtained, for neutrons [14–29], protons, and α particles [30–34]. The rapid mutual Coulomb repulsion experienced by the fission fragments causes a kinematic focusing of light particles emitted from the fragments. This fact allows an angular correlation measurement of the light particles to be decomposed into those particles emitted from the composite (fused) system before scission (pre-scission particles) and those emitted from the fragments (post-scission). The sum of the energy required for the emission of all particles, pre-scission and post-scission, plus that carried away by γ rays and in the TKE of the two massive fragments, allows the reconstruction of the initial excitation energy of the system. For a pure fusion-fission reaction, this should be consistent with the value calculated for the fusion reaction. For most reactions, the TKE and the energy lost due to neutron emission are the dominant contributions.

During the course of a heavy-ion collision, the emission of light particles (principally neutrons, protons, and α particles) will in reality be a continuous process, occurring between the first excitation of the colliding nuclei and the de-excitation of the final products to energies below the respective emission thresholds. The probabilities of emission as a function of time will depend in detail on the dynamics of the reaction process, although the total energy carried away will be determined largely by the reaction Q-value and kinetic energies of the massive fragments. Restricting ourselves to the reactions studied in this work, namely, fusion-fission and quasifission, it is clear that during the course of the reaction, the splitting (scission) of the composite nucleus previously formed by the joining of the projectile and target nuclei represents a unique and irreversible event in the decay history of the reaction, and as such is often the end point of theoretical descriptions of the reaction process [35].

For quasifission, and for composite nuclei with fission barrier less than the temperature ("fast fission"), the probability of not undergoing scission is essentially zero, independent of nuclear viscosity. In these reactions it is clear that fission need not be considered as a decay channel *competing* with evaporation, but rather as a shape change *influencing* the evaporation process. The average trajectory to scission will be determined by the inertia

and nuclear viscosity; thus future developments in the modeling of reaction dynamics and evaporation should allow precise information on the nature and magnitude of nuclear viscosity to be obtained. In fusion-fission (fission with barrier) the treatment of the strong relationship between the fission width and the magnitude of the viscosity [35] (the Kramers factor) causes some problems [20] in reproducing measured fission probabilities. However, the fact that in this class of reaction fission occurs *because* of the coupling between intrinsic and collective degrees of freedom (viscosity) makes the study of fusion-fission particularly important in developing our understanding of fission dynamics.

Experimental studies of the pre-scission particles can be divided into neutron and charged-particle studies. The latter have some difficulties in their measurement and interpretation, namely, (i) the low multiplicity in most reactions, (ii) the strong angular distribution, particularly for α particles, which makes more difficult the extraction of the multiplicity from the angular correlation, and (iii) the sensitivity of the calculated emission widths and thus multiplicities to the deformation of the emitter and to the slope of the yrast line as a function of angular momentum. The latter points can also be exploited to advantage, since in principle they allow the extraction of more information about the emitting system, in particular in conjunction with neutron measurements [34].

Neutron measurements are hampered by the well-known problems of neutron detection, such as the detection efficiency which is usually low and is energy dependent, and small solid angles. Nevertheless, they allow the determination of reaction time scales with arguably less uncertainty than do charged-particle measurements, permit the calculation of the initial excitation energy, and are emitted with high multiplicities.

Pre-scission neutron and charged-particle data for a given reaction all show a multiplicity which increases monotonically with bombarding energy, in contrast with statistical model calculations. This important feature has been explained in terms of the time scale of the fission process, and shows that fission is a slow process ($\gtrsim 10^{-20}$ s) compared with the typical lifetime for emission of the first neutrons ($10^{-22}-10^{-20}$ s). Neutron emission being the dominant decay mode permits an analogy with a clock [26], each additional neutron representing an increment in time from the formation of the thermally equilibrated compound nucleus. As the bombarding (excitation) energy is increased, the first neutron is emitted more and more rapidly; thus if the fission time-scale does not decrease, then most of the increased excitation energy is removed by pre-scission emission, and the temperature of the fission fragments increases only slowly. This fact has important implications in the analysis of measured properties of the fission fragments [26].

Measurements of pre-scission neutron multiplicities (ν_{pre}) in heavy-ion reactions were initially made for fission events without any discrimination in mass split and TKE. Recent measurements as a function of mass split [25] indicate that information on the reaction mechanism in quasifission,and on fission dynamics in fusion-fission, can be extracted from such data. The variation of ν_{pre} with TKE will in principle give information on the reaction mechanism and/or the importance of emission near the scission point, if the kinematical effects due to recoil imparted by the observed neutron are accounted for in the data analysis [29]. Some measurements as a function of the fissility (x) of the compound system have already been made, but analyses to date [24,26] show that the variation of the deduced dynamical fission time scale with fissility depends very much on the assumptions made about the average deformation from which the neutrons are emitted. More precise data are required, together with the development of realistic dynamical models of the fission process which incorporate particle decay, which will allow a direct comparison of experiment and theory without the intermediate step of statistical model codes modified to simulate the effect of dynamics.

In order to further our understanding of the dynamics of nuclear coalescence and separation in fusion-fission and quasifission, a series of measurements of pre-scission and post-scission neutron multiplicities for reactions induced by ^{16,18}O, ^{40}Ar and ^{64}Ni projectiles has been carried out. For many of the reactions, particularly those with wide mass distributions, the variation with mass split and also TKE was measured. In all, 248 data points were analyzed, which represents a considerable increase in the data available up to now.

In one paper, it is not practicable to give a full interpretation of every aspect of these new data. The aim here is to describe the experimental methods used, present the experimental data, and highlight the main trends observed. Our interpretation of these trends will be given together with the problems involved in obtaining definitive quantitative conclusions.

II. EXPERIMENTAL PROCEDURE

The experiments were carried out at the Hahn-Meitner-Institut using pulsed beams of 158.8 MeV ^{18}O, 288.0 MeV ^{16}O, 249.0 MeV ^{40}Ar, and 417.7 MeV ^{64}Ni, from the VICKSI Accelerator, incident on a range of targets. Those measurements using beams of ^{16,18}O and ^{64}Ni were performed using essentially the same experimental configuration, while those using the ^{40}Ar beam had a different arrangement. In the following description, the conditions for the ^{40}Ar measurements will be given first, with the others in parentheses after.

A. Fission fragment detection

Fission fragments were detected in low-pressure position-sensitive multiwire proportional counters [36] (MWPC), shown in Fig. 1. Two (one) small area MWPC's of active area 6.1 cm $\times$6.1 cm were located on one side of the beam, with a distance of 31.1 cm (25.6 cm) between the target and the timing plane. Their angle θ_F could be varied. On the other side of the beam was a large area MWPC (24.4 cm $\times$12.2 cm) centered at 100° (55°), with 18.2 cm (27.1 cm) between target and timing plane. It subtended 67° (48°) in plane and $\pm$18.5° ($\pm$12.7°) out of plane. These detectors provided better than 0.1 cm position resolution and better than 200 ps time resolu-

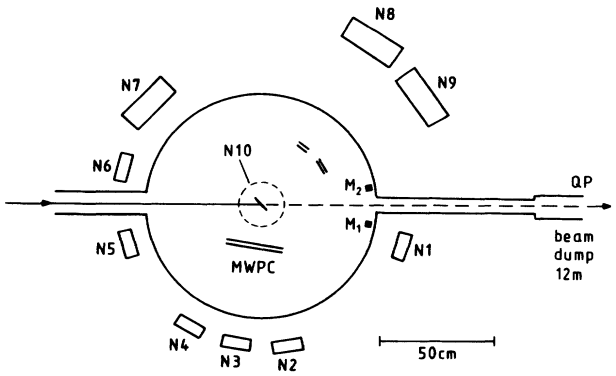

FIG. 1. Schematic diagram of the experimental arrangement for the ^{40}Ar runs; neutron detectors are indicated by $N1$ to $N10$, the latter being out of plane. Monitor detectors $M1$ and $M2$ were near to the beam direction. Fission fragments were detected in the three MWPC detectors, each indicated by a double line. In the other runs, only one small solid angle MWPC was used.

tion. The angle calibrations were carried out using fission fragments, which passed through masks (located on movable arms) previously calibrated in place by a telescope aligned with the beam axis.

Targets were typically 0.3–0.5 mg/cm^2 in thickness, measured in most cases using an α-particle source. The targets were in general not placed with the normal to their surface at 0° to the beam axis, but were turned between 10° and 65°, in order to reduce energy loss and multiple scattering of both fission fragments leaving the target, details for each reaction being given in Tables I–IV. This information was necessary to calculate the mean beam energy in the target for each reaction, and to calculate the mean velocity of elastically scattered beam particles and recoils exiting the target at all angles. The latter were used to determine the time of arrival (t_0) of the beam pulses (of width $\lesssim$200 ps for the ^{18}O beam to 1.6 ns for ^{64}Ni) at the target in those reactions where elastic-recoil coincidences were observed. It was found that changes of t_0 from reaction to reaction as determined by this method were in excellent agreement with changes determined from the shift in the time of arrival of γ rays at the neutron detectors. When the former method could not be used, t_0 was determined from the γ peak in the neutron detectors, with an error estimated to be less than $\pm$150 ps.

Having both t_0 and the angle calibration, the velocity vectors $\mathbf{v}_{F_1}$ and $\mathbf{v}_{F_2}$ of each fragment were determined, and as described in Ref. [27], the mass split, center-of-mass velocity v_0, and the total kinetic energy (TKE) were determined, an iterative procedure being used to compensate for the energy loss in the target. Movement of the beam spot was monitored by a pair of plastic scintillator detectors (M_1 and M_2 in Fig. 1) at $\pm$11° in-plane, and was accounted for in determining $\mathbf{v}_{F_1}$ and $\mathbf{v}_{F_2}$. For the ^{64}Ni beam, the poorer beam pulse width resulted in degraded TKE resolution. For these reactions, it was found as expected that v_0 was consistent with the value calculated for complete momentum transfer, so v_0 was fixed to these values, thus allowing the TKE to be determined with better precision. Depending on the reaction, a cut of between $\pm$0.08 and $\pm$0.15 cm ns^{-1} was applied around the measured v_0. In all cases, a cut of between $\pm$6.5° and $\pm$15° was applied about 180° to the out-of-plane correlation. These helped to restrict the events to binary fission, and to exclude fission following momentum transfers substantially less than average. In addition, generous cuts were applied to the energy loss (ΔE) signal in the MWPC's and to the relative velocity between the two fragments. These measures resulted in extremely clean fission fragment spectra.

The main sources of systematic uncertainty in the extracted mass split and TKE information are the uncertainty in target thickness and beam spot position, and the uncertainty in t_0 for each detector. The resulting systematic uncertainty in fragment mass is $\lesssim\pm$2% and in TKE $\lesssim\pm$3%. The resolution in mass due to time and position resolution of the detectors was typically $\lesssim\pm$1%, and in TKE $\lesssim\pm$4%, substantially smaller than the cuts applied to the data. These figures are excellent for the purposes of these measurements, although if a detailed investigation of fission mass and TKE distributions were to be carried out, they could be considerably improved by using thinner targets and different geometry, though at the expense of yield. It should be further noted that the fission fragment yields shown have not been corrected for efficiencies caused by the detector geometry and kinematics.

B. Neutron detection

Liquid scintillator neutron detectors (NE213 or BC501) were placed outside the 1 m diameter scattering chamber (Fig. 1), whose walls were of 0.3 cm thick stainless steel. In the ^{40}Ar measurements, 10 neutron detectors were used ($N1$ to $N10$ in Fig. 1), and 12 in the other measurements. Detector sizes were 10.16 cm in diameter $\times$10.16 cm in length, 12.7 cm $\times$5.08 cm, 25.4 cm $\times$5.08 cm, and 25.4 cm $\times$10.16cm. They were placed both in plane and out of plane at distances ranging from 65 to 105 cm for backward and forward angles, respectively.

TABLE I. Target properties and detector angles for the reactions with 158.8 MeV ^{18}O.

Target material	$^{nat}UF_4$	^{197}Au	^{169}Tm	^{154}Sm	^{144}Sm	^{124}Sn
Thickness (mg/cm^2)	0.27	0.31	0.39	0.40	0.75	1.66
Target angle (deg)	60	60	45	60	60	60
E_{lab} (MeV)	158.5	158.4	158.5	158.3	157.8	156.4
θ_F (deg)	−95	−90	−90	−80	−80	−75
θ_n (deg)	−90	−90	−90	−80	−80	−70

TABLE II. Target properties and detector angles for the reactions with 288.0 MeV ^{16}O.

Target material	$^{nat}UF_4$	^{208}Pb	^{197}Au	^{184}W	^{154}Sm	^{109}Ag
Thickness (mg/cm^2)	0.27	0.22	0.28	0.50	0.40	0.16
Target angle (deg)	60	60	60	60	65	25
E_{lab} (MeV)	287.8	287.8	287.7	287.5	287.5	287.9
θ_F (deg)	−90	−85	−80	−75	−65	−45
θ_n (deg)	−90	−85	−80	−75	−65	−59

Time resolution of the detectors varied from 0.9 to 2.0 ns, depending on their size and lower threshold setting. Neutrons were identified by their time of flight and by pulse-shape discrimination. Comparison of the deposited energy as determined by a γ-ray source calibration, and the true energy as determined from the time of flight, allowed the rejection of scattered events with long times but high energies. The efficiencies of the neutron detectors were determined three times *in situ* using a ^{252}Cf source mounted in a lightweight MWPC at the target position, supplemented for high neutron energies by calculated values from a Monte Carlo code [37]. Thus to first order, the effect of neutron scattering into the detectors, which was not rejected by the method described above, was accounted for. This procedure also accounts for the energy-dependent reduction of neutron intensity by the experimental apparatus, vacuum chamber wall, and the 7 mm of lead placed in front of the neutron detectors to reduce the γ-ray rate. Additional effects accounted for in the measurement of the neutron spectra were (i) random coincidences, which were measured two beam bursts later ($\sim$270 ns) than the fission fragments, and constituted 0.5–2% of the true events; (ii) blocking of neutrons by γ rays from the observed fission event ($\lesssim$2%); (iii) dead time in each of the neutron-gamma discriminator units, in the range 1–6%; and (iv) the neutron velocity-dependent "blocking" of slower neutrons by faster neutrons incident on the same detector—experimentally the flight time measured is always that of the faster neutron. This was corrected for exactly by an "inverted spectrum stripping" procedure applied to each measured spectrum. This was started at the highest velocity (energy) bin, where no increase in yield was applied, at the next lowest velocity bin, the blocking due to the higher bin was calculated and the measured yield increased slightly, and so on, with the effect building up to a maximum of a 10% increase in yield at the lowest velocity in the detector with the highest yield (120 msr solid angle coaxial with the direction of the forward-going fission fragment). Account was also taken of the probability that both neutrons may be rejected as a scattered event by appearing to deposit too high an energy; this effect is small except where both neutrons have a similar velocity, where this correction approaches 50%. Finally, (v) the velocity resolution caused by the finite thickness of the neutron detectors and their time resolution was not unfolded, but was rather folded in during the fitting procedure described below.

All the measures described above enabled reliable neutron spectra to be obtained for detectors with relatively large solid angle, thus enabling good statistics to be obtained (nearly 10^7 fission-neutron coincidences in 48 hours for the ^{40}Ar+^{238}U reaction).

In the ^{40}Ar run, the two neutron detectors behind the small MWPC's were moved together with the MWPC's, so as to remain most sensitive to the post-scission neutrons. Their angles are indicated in Table III by θ_n and θ_F, respectively. In the other runs, a group of four detectors was moved as the small MWPC was moved, to retain sensitivity to the post-scission neutrons emitted by the fragment detected in that MWPC. The angle of the central detector is given in Tables I, II and IV by θ_n.

III. DATA ANALYSIS

A. Fission fragments

As described, measurement of the velocity vectors of the two fission fragments enables the fragment mass ratio ($R_F = A_1/A_2$) at scission to be determined, under the assumption that the mean fragment velocities are unchanged during their decay. For convenience in presenting the data, the mass ratio has been converted into a fragment mass assuming no particle emission, thus

$$A_1 = \frac{A(\mathrm{CN})R_F}{(1+R_F)} ,$$

where A(CN) is the compound nucleus mass number. Similarly, to enable comparison with the Viola systematics [38], the TKE has been determined from the masses

TABLE III. Target properties and detector angles for the reactions with 249.0 MeV ^{40}Ar.

Target material	$^{nat}UF_4$	^{208}Pb	^{197}Au	^{181}Ta	^{165}Ho	^{169}Tm	^{141}Pr
Thickness (mg/cm^2)	0.27	0.22	0.50	0.54	0.50	0.50	0.60
Target angle (deg)	60	60	60	60	60	60	60
E_{lab} (MeV)	246.8	246.5	245.9	245.4	245.6	245.6	244.5
θ_F (deg)	−24, −34	−24,	−24,	−24,	−24,	−24,	−24,
	−46, −56	−46	−46	−46	−46	−46	−46
θ_n (deg)	−24, −35	−24,	−24,	−24,	−24,	−24,	−24,
	−45, −57	−45	−45	−45	−45	−45	−45

TABLE IV. Target properties and detector angles for the reactions with ^{64}Ni.

Target material	$^{nat}UF_4$	^{208}Pb	^{197}Au	^{175}Lu	^{154}Sm
Thickness (mg cm^{-2})	0.68	0.70	0.28	0.47	0.40
Target angle (deg)	65	60	60	60	90
E_{lab} (MeV)	410	410	415	412	413
θ_F (deg)	−57	−50	−50	−50	−50
θ_n (deg)	−55	−55	−55	−55	−55

A_1 and A_2 defined above, and the measured fragment velocities. Thus A and TKE in the tables and figures do not represent exactly the actual masses and energies of fragments incident on the detectors. Fragments from symmetric fission appear to have a mass of half the compound nucleus mass.

Gates were applied to the fission mass spectrum in order to determine the mass-asymmetry dependence of neutron multiplicities. However, to make straight cuts in TKE would have resulted in different mass yields for each TKE gate. Thus a new quantity was generated, the ratio of the measured TKE to that calculated from the Viola systematics, with the mass-asymmetry dependence included [21], which we will denote by RTKE, given by

$$\mathrm{RTKE}=\frac{\mathrm{TKE}(R_F)}{[0.755Z_1Z_2/(A_1^{1/3}+A_2^{1/3})]+7.3} \quad (1)$$

It was assumed that the Z/A ratio of the fragments is the same as that of the compound system. Linear cuts in RTKE were applied to the fragments; the appearance of such gates is shown in Fig. 10.

B. Neutrons

One neutron detector was placed at 90° out of plane, the others were in plane or slightly out of plane ($<25°$) to avoid obstacles. The former detector allowed testing of the assumption of isotropic neutron emission. Since pre-equilibrium neutrons were not of primary interest, fitting of the neutron spectra was performed in velocity space, which is convenient for presentation and evaluation of fits.

The neutron angular correlations were fitted as a function of neutron velocity using a multiple-source-fitting program similar to that of Ref. [24]. The philosophy was to generate trial spectra, and calculate the χ^2 value for all combinations of multiplicities. New trial spectra were then taken and the procedure continued until the χ^2 surface was mapped out, the minimum χ^2 found and the locus of lowest χ^2 values for each parameter, determined for free variation of all other parameters. This gave the best-fitting value of each parameter, and its uncertainty, a 70% confidence level being associated with a value of χ^2 per point higher than the minimum value by 0.03, the appropriate value for the number of data points fitted, assuming that the experimental errors are solely due to statistical fluctuations in the neutron spectra collected. The influence of systematic uncertainties will be discussed in Sec. IV.

The basic assumption in generating the trial spectra was that neutrons are emitted sequentially, each with an energy spectrum $d\sigma/dE_n$ of Maxwellian form, given for neutron i by

$$\frac{d\sigma}{dE_n}=\frac{E_n}{T_i^2}\exp(-E_n/T_i)\ ,$$

where T_i is determined by the thermal excitation energy E_i and the level density parameter a_n ($T_i=\sqrt{E_i/a_n}$). Thus starting at an initial thermal energy E_1, the mean value of E_2 was given by $E_2=E_1-B_1-2T_1$, where B_1 is the neutron binding energy. Support for the use of Maxwellian spectra comes from the results of statistical model calculations [27], and the excellent quality of the fits obtained to the experimental angular correlations (see also Sec. IV A 1).

Four sources were assumed: two fission fragments moving with their average measured velocity vectors corrected for energy loss in the target, the compound system moving with the mean experimentally determined velocity v_0, and a pre-equilibrium source moving with half the beam velocity. The latter spectrum was taken to be a single Maxwellian distribution with characteristic temperature, which was a free parameter as was the multiplicity ν_{pee}. The pre-scission source was taken as a single Maxwellian for the ^{40}Ar data, or a number of Maxwellian spectra emitted from a starting energy E_{pre} over an energy range ΔE_{pre}. E_{pre} and the multiplicity ν_{pre} were varied in the fit, there was little sensitivity to ΔE_{pre}, and a reasonable value was chosen depending on the value of ν_{pre}. The post-scission sources were represented by a number of Maxwellians starting at energies E_{post_1} and E_{post_2} for each fragment, and ending at 2 MeV; this value was not very critical, and was estimated from the quality of the fits at $v_n \simeq v_F$. The use of Watt spectra to represent the post-scission sources resulted in severe overestimation of the observed yield at $v_n \simeq v_F$. E_{post_1} and E_{post_2}, and the multiplicities ν_{post_1} and ν_{post_2}, were varied in the fitting. It was assumed that neutrons were emitted isotropically in the center-of-mass frame of each source, which has not yet been contradicted in measurements [18], except for pre-equilibrium neutrons at beam velocities higher than used here [18]. For whatever gate was applied to the fission fragments, the fragment mean velocities $\bar{v}_{F_1}$, $\bar{v}_{F_2}$, and their rms deviations $\sigma_{v_{F_1}}$, $\sigma_{v_{F_2}}$, mean fragment angles $\bar{\theta}_1$, $\bar{\theta}_2$, and the rms deviations in θ_1,θ_2 ($\sigma_{\theta_1},\sigma_{\theta_2}$) and ϕ_1,ϕ_2 ($\sigma_{\phi_1},\sigma_{\phi_2}$) were taken from the measurement and accounted for in the fitting program. For different reactions, fits were made to all fissions, to mass cuts and RTKE cuts, and to RTKE cuts applied to given mass re-

gions. In all, fits were made to 248 angular correlations from 27 different reactions.

IV. EXPERIMENTAL RESULTS AND INTERPRETATION

The experimental results will be presented in four sections. Section A comprises the fusion-fission reactions induced by the ^{16,18}O projectiles. Section B present the pre-scission neutron data for the ^{40}Ar-induced reactions, having some quasifission component. Section C discussed the data obtained for quasifission, using the ^{64}Ni projectile. Finally, Sec. D contains a discussion of the post-scission neutron multiplicities from all reactions.

A. ^{16,18}O-induced reactions

The data and discussion for fission events without mass or RTKE gates applied will be given first, followed by those for fission with gates applied.

1. All fission

The measured characteristics of the singles fission events observed in the reactions of 158.8 MeV ^{18}O with ^{238}U, ^{197}Au, ^{169}Tm, ^{154}Sm, ^{144}Sm, and ^{124}Sn are shown in Table V. The mean and variance of the mass and TKE distributions are for convenience calculated from the measured fragment velocities assuming no particle evaporation. The values for the ^{124}Sn target will have the greatest uncertainty, due to the thickness and nonplanarity of the target. Comparison of the measured TKE values with those expected from the Viola systematics [38] shows agreement within the likely systematic uncertainties. Table V shows the deduced neutron multiplicities for each reaction, comprising pre-equilibrium (ν_{pee}), pre-scission ($\nu_{\rm pre}$), post-scission from both fragments ($2\nu_{\rm post}$), and the total evaporated (equilibrium) multiplicity $\nu_{\rm tot}=\nu_{\rm pre}+2\nu_{\rm post}$. In fitting these data, the characteristics of the post-scission sources were constrained to be the same. Also shown in the table are the mean kinetic energies of the prescission neutrons ε_ν. The data for the 288 MeV ^{16}O-induced reactions are shown in Table VI.

The main features of the multiplicity data are shown in Fig. 2 as a function of the mass number of the compound nucleus A(CN). It is clear that the extra excitation energy brought in by the 288 MeV ^{16}O beam is largely removed by pre-scission emission, while the post-scission multiplicity is almost unchanged, in agreement with previous conclusions [26].

The experimental uncertainties quoted here and later are those derived from the χ^2 analysis described in Sec. III B. To investigate the relative significance of random and systematic errors, the data for the ^{18}O+^{197}Au reaction were split into nine equal sections, and each was sorted and fitted independently. The scatter on all the fit parameters was consistent with a random error due to statistical fluctuations in the spectra about a factor of 4 smaller than the error derived from the χ^2 analysis. This can be explained by degradation of the quality of the fit by systematic errors, which are likely to be largely due to uncertainty in the relative efficiencies of the neutron

TABLE V. Neutron multiplicities and statistical-model input parameters for the reactions of 158.8 MeV ^{18}O. The critical angular momentum for fusion ($l_{\rm fus}$) is calculated from the fusion cross-section assuming a sharp cutoff. In the statistical-model calculations, an appropriate smooth cutoff was used.

Target	A(CN)	A(CN) a_ν	$\sigma_{\rm fus}$ (mb)	$l_{\rm fus}$	E_x (CN)[a] (MeV)	ν_{pee}[b] (error)	ΔE_{pee} (MeV)	$\nu_{\rm pre}$ (error)	ε_ν (MeV) (error)	$\nu_{\rm post}$ (error)	$\nu_{\rm tot}$ (error)	σ_A[c]	TKE (MeV)	$\sigma_{\rm TKE}$[d] (MeV)
^{238}U	256	8.96	1750	81	101.2	0.37 (0.20)	3.1	5.10 (0.25)	3.30 (0.10)	4.25 (0.15)	13.60 (0.20)	23.3	181	20.5
^{197}Au	215	8.86	1680	78	111.1	0.30 (0.15)	3.2	4.10 (0.15)	3.35 (0.08)	2.70 (0.10)	9.50 (0.10)	16.5	154	13.8
^{169}Tm	187	8.60	1700	77	115.0	0.30 (0.15)	4.7	3.70 (0.30)	3.56 (0.12)	2.25 (0.10)	8.20 (0.13)	14.8	128	11.2
^{154}Sm	172	8.50	1700	76	120.8	0.20 (0.10)	5.7	4.40 (0.15)	3.53 (0.08)	2.00 (0.05)	8.40 (0.12)	15.1	113	10.6
^{144}Sm	162	8.43	1600	73	113.6	0.20 (0.10)	4.2	2.45 (0.25)	3.70 (0.08)	1.70 (0.15)	5.85 (0.20)	15.2	112	
^{124}Sn	142	8.26	1750	75	121.5	0.18 (0.10)	6.8	2.90 (0.25)	3.60 (0.18)	1.75 (0.10)	6.40 (0.14)	16.4	81	

[a]Excitation energy above the liquid-drop ground state, the calculated energy removed by pre-equilibrium neutrons and protons (ΔE_{pee}, see column 8) is already subtracted.
[b]Pre-equilibrium neutron multiplicity, for an effective temperature in the fitting program of 2.5±0.5 MeV.
[c]rms deviation of the fission mass distribution.
[d]rms deviation of the fission TKE distribution, for all masses.

detectors. To test this hypothesis, an additional error of 2% was added linearly to the statistical error of each point in each neutron velocity spectrum, to represent the estimated uncertainty in the efficiencies. This gave the same best-fitting multiplicities as previously, with χ^2 per point values around unity for all cases investigated, but resulted in larger deduced error bars, due of course to the greater freedom allowed by the larger assigned uncertainty in the raw data. It is to be expected that systematic uncertainties of this order (which are almost impossible to measure) will be present in the efficiencies, however, it seems reasonable to assume that, with 10 or 12 neutron detectors, these small systematic errors are unlikely to bias the deduced multiplicities significantly. Thus, in particular when looking at relative shifts in multiplicity, we may be justified in taking a smaller random error than those quoted. This is only done, however, in the interpretation of the results for the $^{40}Ar+^{238}U$ reaction in Sec. IV B 2. In all other cases the uncertainties deduced from the χ^2 analysis are used.

Part of the overall 2% deviation between fits and data may be due to the possibility that the trial spectra are not correct at this level. Because of the inevitability of systematic uncertainty in the neutron detector efficiencies, it can thus be concluded that the uncertainty due to the choice of the form of the trial spectra is of this order or smaller.

In making a more quantitative analysis of these data, several parameters must be defined. The first is the fusion cross section (σ_{fus}). For the 158.8 MeV ^{18}O reactions, experimental data [39] and the predictions of the Bass model [40] were used to determine the cross sections given in Table V. For the 288 MeV ^{16}O reactions, interpolation of experimental results for a number of targets [41] and scaling from the measured yields for the ^{18}O data enabled estimates of σ_{fus} to be made (Table VI). The second parameter is the initial thermalized excitation energy of the compound nucleus E_x(CN), that is, after energy removal by pre-equilibrium emission and/or incomplete fusion. The pre-equilibrium neutron multiplicity was measured, and with the help of the Boltzmann master equation computer code BME [42], estimates of the pre-equilibrium proton multiplicity and the total energy removed by pre-equilibrium particles were made (see Tables V and VI). No measurements were made of the contribution due to fission following incomplete fusion due to the massive transfer mechanism, however, an asymmetry in the deduced center-of-mass velocities (v_0) to lower velocities was observed for the heaviest targets when bombarded by 288 MeV ^{16}O, so some further reduction in excitation energy may be expected; however, at this stage, without any quantitative information, no correction for fission following incomplete fusion was applied. The values of E_x(CN) used in calculations were as shown in Tables V and VI.

At this stage, it is useful to show a comparison between the measured values of ν_{tot} and those calculated using a heavily modified version of the computer code JULIAN [27]. The calculation involved reproducing the measured values of ν_{pre} and ε_ν as will be described later. The evaluation of ν_{post} was performed as described in Ref. [27],

TABLE VI. Neutron multiplicities and statistical-model input parameters for the reactions of 288.0 MeV ^{16}O.

Target	A(CN)	$\frac{A(CN)}{a_\nu}$	σ_{fus} (mb)	l_{fus}	E_x(CN)[a] (MeV)	ν_{pee}[b] (error)	T_{pee}[c] (MeV)	ΔE_{pee} (MeV)	ν_{pre} (error)	ε_ν (MeV) (error)	ν_{post} (error)	ν_{tot} (error)	TKE (MeV)	σ_{TKE}[d] (MeV)
^{238}U	254	8.95	1550	97	191.9	0.95 (0.20)	3.5 (0.7)	34.7	9.0 (0.5)	4.03 (0.20)	4.45 (0.20)	17.9 (0.3)	184	25.1
^{208}Pb	224	8.82	1600	98	187.3	0.87 (0.15)	3.7 (0.5)	31.7	6.9 (0.3)	4.50 (0.11)	3.40 (0.15)	13.7 (0.2)	166	16.6
^{197}Au	213	8.75	1700	101	191.4	0.95 (0.15)	4.2 (0.5)	35.5	7.2 (0.2)	4.64 (0.15)	2.80 (0.15)	12.8 (0.2)	151	18.2
^{184}W	200	8.68	1400	91	195.8	1.13 (0.15)	4.3 (0.4)	37.5	7.7 (0.3)	4.58 (0.12)	2.65 (0.15)	13.0 (0.2)	139	16.5
^{154}Sm	170	8.49	1300	86	205.8	0.85 (0.20)	5.0 (1.0)	43.0	8.4 (0.4)	4.87 (0.16)	1.85 (0.20)	12.1 (0.2)	111	14.5
^{109}Ag	125	8.12	1200	80	194.1	1.00 (0.20)	5.0 (1.5)	49.2	4.0 (0.5)	4.80 (0.20)	1.13 (0.15)	6.25 (0.30)	77	15.0

[a]Excitation energy above the liquid-drop ground state, the calculated energy removed by pre-equilibrium neutrons and protons (ΔE_{pee}, see column 8) is already subtracted.
[b]Pre-equilibrium neutron multiplicity, for an effective temperature in the fitting program of T_{pee}.
[c]Fitted pre-equilibrium neutron temperature (see text).
[d]Measured rms deviation of the fission TKE distribution, for all masses.

with mass split and TKE chosen randomly for each of 10 000 events so as to reproduce the measured distributions. The level density parameter used for the fragments was that for a symmetric split, calculated according to Tōke and Swiatecki [43]. Figure 3 shows the comparison between experiment and calculation, the uncertainty in the calculation due to the systematic error in the measured TKE being larger than the statistical uncertainty in the ν_{tot} data. For the 158.8 MeV ^{18}O-induced reactions, the agreement is generally good, except for the heaviest targets, where some effect of fission following incomplete fusion is likely, and will result in a lower measured total multiplicity than calculated. For the 288 MeV ^{16}O reactions (see Fig. 4) the results are qualitatively similar, a discrepancy only occurring for the heaviest systems, consistent with the observations of v_0 noted above.

Having fixed the initial excitation energy (with some uncertainty), the next step is the interpretation of the pre-scission data. It is now well established that fission is a slow process, taking several 10^{-20} s. Except at low excitation energies [19,26], this time is longer than the statistical model lifetime τ_{sm}, which means that before the decision to fission is made, a number of particles in addition to those predicted by the statistical model may be evaporated. These are usually predominantly neutrons. The number of particles of type i evaporated in a given time can be determined if their decay widths Γ_i are calculated, thus allowing the lifetime for particle emission $\tau_j = \hbar/\sum\Gamma_{ij} = \hbar/\Gamma_{tot_j}$ to be calculated at each decay step (j). Where neutrons are predominant, the pre-scission neutrons may be thought of as a clock, measuring the time between thermal equilibration and scission (τ). The total fission time scale τ is made up of the dynamical time

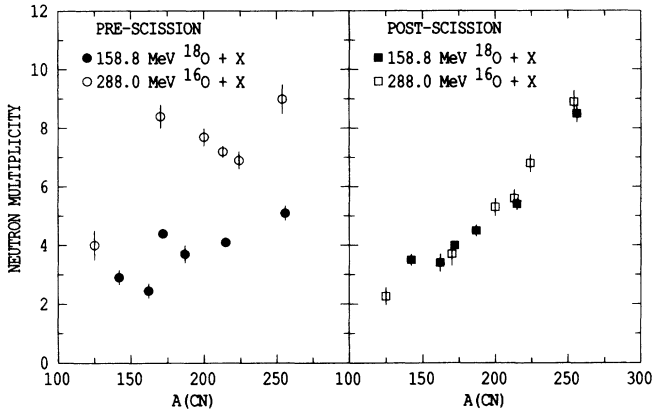

FIG. 2. Measured ν_{pre} and $2\nu_{post}$ (post-scission multiplicity for both fragments) values for the ^{18,16}O reactions as a function of the compound nucleus mass number. It is clear that almost all of the extra energy brought in by the higher energy ^{16}O projectile is removed by pre-scission emission, since the post-scission multiplicity is almost unchanged.

scales, namely, the pre-saddle delay time τ_d and the saddle-to-scission time τ_{ssc}, and the statistical model time τ_{sm}. Thus for a given nucleus

$$\tau = \tau_d + \tau_{sm} + \tau_{ssc} = \sum_{j=1}^{j=\infty} t_j W_j \ ,$$

where t_j are the decay times at step j randomly distributed with characteristic lifetime τ_j, and appropriate weighting of decay steps (W_j) reproduces the measured ν_{pre}. W_j represents the probability that scission will

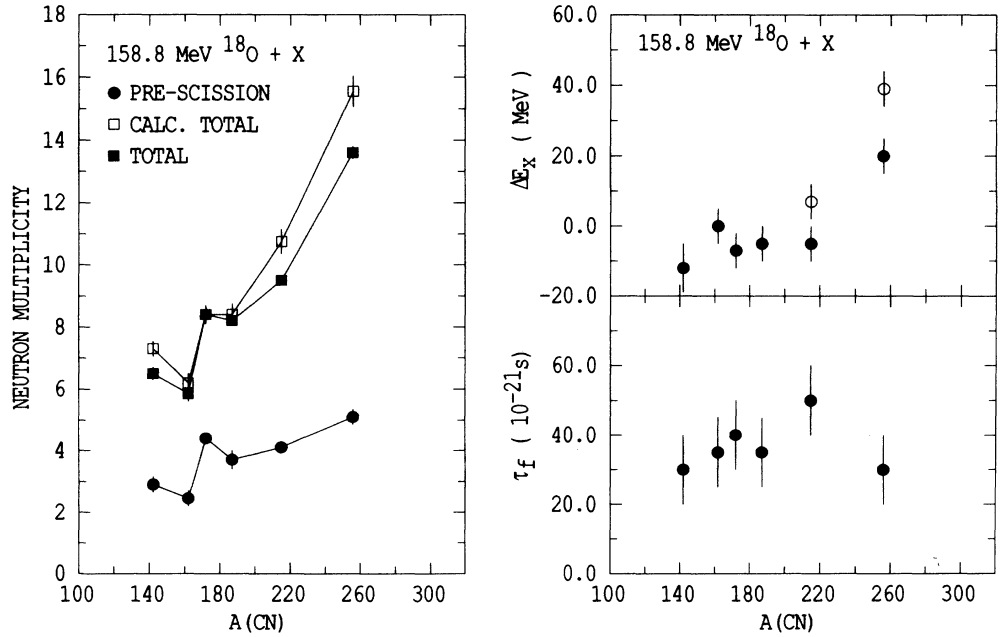

FIG. 3. The left panel shows the measured ν_{pre} and ν_{tot} values for the 158.85 MeV ^{18}O-induced reactions, together with the calculated ν_{tot} values discussed in the text. The right panels show the deduced values of τ_f and ΔE_x, using the initial excitation energies given in Table V (solid points), and using a reduced value to give consistency between measured and calculated ν_{tot} values (outline points).

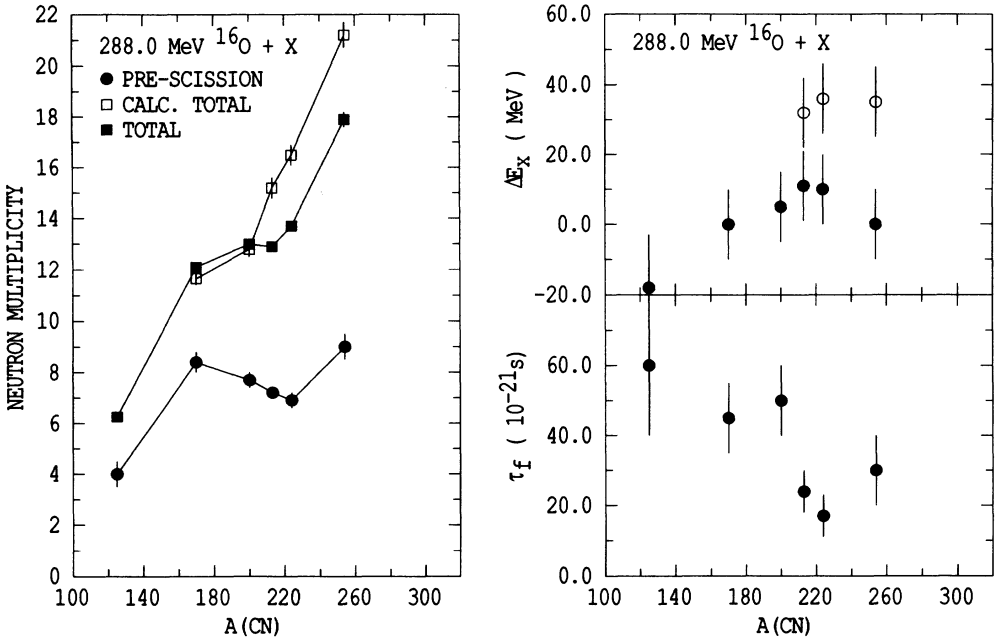

FIG. 4. As Fig. 3, but for the reactions induced by the 288.0 MeV ^{16}O beam.

occur at a later step than j: in the simplest approximation, and if $\nu_{\rm pre}$ is integer, $W_j=1$ for j less than or equal to $\nu_{\rm pre}$. For an ensemble of nuclei, the value of $\nu_{\rm pre}$ can then be mapped directly to τ, and as $\tau_{\rm sm}$ is small for these reactions, yields the dynamical time scale $\tau_f=\tau_d+\tau_{\rm ssc}$. The time for formation of the composite system at the equilibrium deformation, assuming that this occurs after thermal equilibration, will be included in τ_d.

In the computer code JULIAN, which models the statistical decay of nuclei, it is possible to totally suppress the fission width for a given time. During this time, particle evaporation is allowed, corresponding to emission from the equilibrium deformation; thus strictly this time should most closely correspond to the delay time τ_d. However, it will be shown that even without theoretical knowledge of the trajectory in deformation space, τ_f can be determined to first order from $\nu_{\rm pre}$. The time delay in JULIAN will be referred to as τ_f.

Calculation of the "neutron clock rate" requires the determination of the absolute decay width Γ_ν as a function of the excitation energy (E) and angular momentum (I) of the compound system. This is given by [27]

$$\Gamma_\nu(E_x,I)=\frac{(2s_\nu+1)}{2\pi\rho(E,I)}\sum_{l=0}^{\infty}\sum_{J=|I-l|}^{J=|I+l|}\int_0^{E-B_\nu}\rho(E-B_\nu-\epsilon_\nu,J)T_l(\epsilon_\nu)d\epsilon_\nu\ ,$$

where s_ν is the spin, l is the orbital angular momentum carried by the neutron, ϵ_ν is the kinetic energy, and B_ν is the binding energy. The uncertainty in calculating Γ_ν lies in determining the ratio of level densities $\rho(E-B_\nu-\epsilon_\nu,J)/\rho(E,I)$ and the transition coefficients $T_l(\epsilon_\nu)$. The level density is taken to have the form

$$\rho(E,I)\propto\frac{(2I+1)}{(E-E_{\rm rot})^2}\exp[2\sqrt{a_\nu(E-E_{\rm rot})}]\ ,$$

where $E_{\rm rot}$ is the energy tied up in rotation of the nucleus and a_ν is the level density parameter. Due to the exponential factor, the greatest uncertainties in Γ_ν are caused by uncertainty in a_ν and in the thermal excitation energy ($E-E_{\rm rot}$). During the fission process, the nucleus passes over the potential energy surface (PES), which varies substantially in height between the equilibrium deformation and scission; thus the thermal excitation energy E_x will vary from that at the equilibrium deformation [E(CN)]. This is shown schematically in Fig. 5 for both light and heavy nuclei. Particularly for the latter, E_x may be very different from E_x(CN); for the ^{40}Ar+^{238}U reaction, neutron lifetimes are calculated to be $\sim$10 times shorter at the scission configuration, only considering the difference in excitation energy. The question is, what values of E_x are appropriate, and without *a priori* knowledge of the trajectory over the PES, the uncertainty in E_x for heavy systems would give little chance of reliably using the neutron clock.

Information on the nuclear temperature ($T=\sqrt{E_x/a_n}$) is, however, carried by the neutron energy spectrum; it is well known that the high-energy slope of an evaporation spectrum can be used to determine the T of the source. In the present measurements we use the experimental mean pre-scission neutron energy ε_ν which

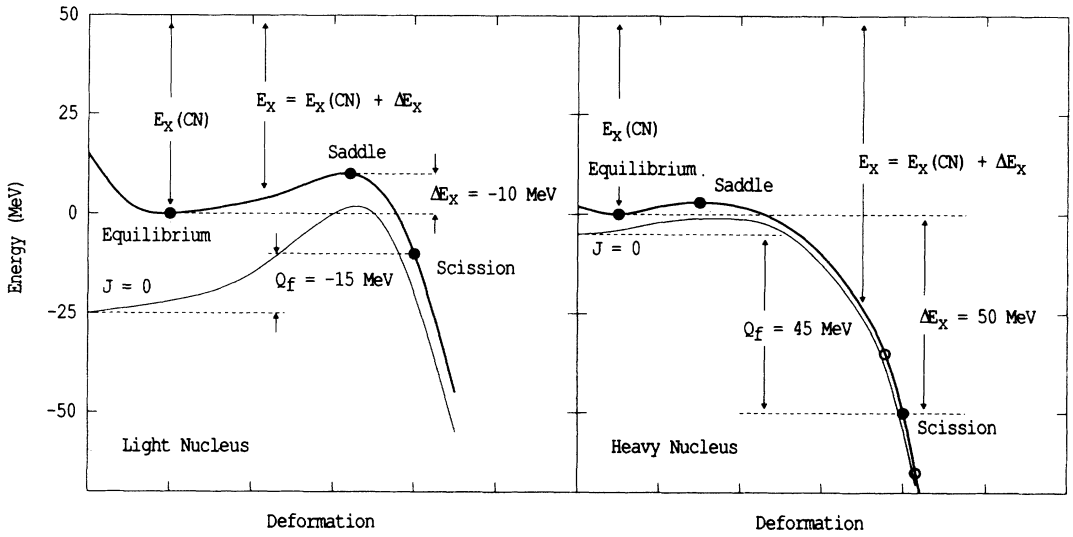

FIG. 5. The potential energy surfaces (PES) of a light and heavy nucleus shown schematically as a function of an aribitrary deformation coordinate which corresponds to the lowest path between equilibrium and scission. The PES for zero angular momentum ($J=0$) and for a typical fissioning angular momentum (heavy line) are shown. The definition of ΔE_x and Q_f are shown. It is clear that on the path to scission, ΔE_x should on average be expected to be negative for the light nucleus and positive for the heavy nucleus.

theoretically is given by

$$\varepsilon_\nu = \sum_{j=1}^{\infty} W_j \frac{\int_0^{E_\nu - B_\nu} \epsilon_\upsilon \Gamma_\nu(E_x, I, \epsilon_\nu) d\epsilon_\nu}{\Gamma_n(E_x, I)} ,$$

where the weighting factor W_j for decay step j has already been defined. Thus by making use of both $\nu_{\rm pre}$ and ε_ν, more accurate conclusions regarding lifetimes should be obtainable.

Within the code JULIAN, where it is assumed that a cascade of neutrons originates from a given initial E_x, that value was adjusted from the calculated E_x^0 (determined by the fusion Q value) by an energy shift ΔE_x, such that $E_x = E_x^0 + \Delta E_x$. Alternatively, variation of a_n would have the same effect on T, and thus on ε_ν; however, because of the uncertainty in E_x due to the PES, a_ν was fixed, the equation of Ref. [43] being used to define it for each compound nucleus (thus it varied over the range $a_\nu = A/8.12$ to $a_\nu = A/9.15$). Extensive calculations have been made for the reaction of 158.8 MeV $^{18}O + ^{154}Sm$ to explore quantitatively the above ideas. For a given ΔE_x, values of $\nu_{\rm pre}$ and ε_ν were calculated for $\tau_f = 0, 10, 20, 50, 100, 200 \times 10^{21}$s; a_ν and a_f/a_ν took values calculated using the expressions of Ref. [43]. The result is shown in Fig. 6, where lines connecting the points show the locus of constant ΔE_x and constant τ_f values. The experimental limits to $\nu_{\rm pre}$ and ε_ν are shown by the vertical and horizontal lines, with the intersection area shaded. Clearly, severe bounds are placed on τ_f and ΔE_x, namely, $30 \times 10^{-21} < t_f < 55 \times 10^{-21}$ s and $-11 < \Delta E_x < -2$ MeV. The use of a fixed value of a_f/a_ν of 1.05, and a value of $a_\nu = A/8.5$ (the value of Ref. [43] for the spherical ^{170}Yb compound nucleus) for $\tau_f = 20$ and $\Delta E_x = 0$, results in a small shift to the circled point, giving a time shift of $<20\%$. The effect of using $a_\nu = A/7.5$ (square point) is to shift ΔE_x by 9 MeV, but there is no time shift; the point lies on the same line of constant τ_f as the circled point with $a_\nu = A/8.5$. In conclusion, there is a slight sensitivity to a_f/a_ν, through the dependence of $\nu_{\rm pre}$ on a_f/a_ν in the statistical model ($\tau_f = 0$), and through the effect of a_f/a_ν on fission probabilities. Variation of a_ν alone is equivalent to changing ΔE_x, within the statistical uncertainty of the Monte Carlo calculation. Thus if one of the three parameters ΔE_x, a_ν, and τ_f is fixed, the other two can be determined by a measurement of $\nu_{\rm pre}$ and ε_ν. Most importantly, as τ_f is of greatest interest, any reasonable combination of ΔE_x and a_ν used will give the correct τ_f if the measured values of both ε_ν and $\nu_{\rm pre}$ are reproduced. The effect of the variation of optical model parameters on $T_l(\epsilon_\nu)$ and subsequently on ε_ν and τ_f is beyond the scope of this paper,

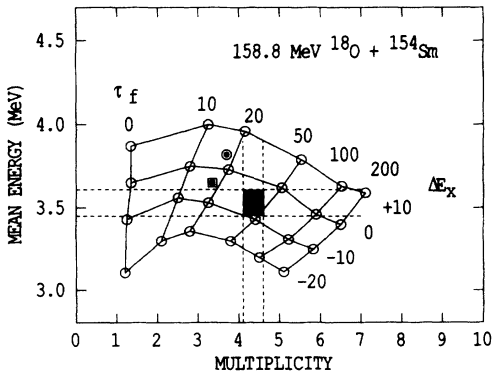

FIG. 6. Calculated correlated values of $\nu_{\rm pre}$ and ε_ν for the reaction indicated, for a variation of τ_f between 0 and 200×10^{-21} s, and for ΔE_x between -20 and $+10$ MeV. The experimental datum is indicated by the black rectangle. Using different level density prescriptions shifts the point at $\tau_f = 20$, $\Delta E_x = 0$ to the outlined circle, and to the outlined square; however, there is little shift in τ_f (see text).

but for neutrons is not expected to be greater than other uncertainties mentioned.

The other experimental data points have been analyzed in a similar way, using the angular momentum dependent a_ν and a_f/a_ν of Ref. [43]. In principle, through the dependence of a_ν on deformation, there will be a relationship between ΔE_x and a_ν; however, for simplicity we have initially fixed a_ν to the value appropriate for a spherical emitter. It was decided to fix a_ν, rather than ΔE_x, because in the fission process, the nucleus moves to the saddle point, losing thermal energy $\Delta E_x(t)<0$, then descends to scission, generally with $\Delta E_x(t)>0$, as is illustrated in Fig. 5. Thus it is not clear which is the appropriate excitation energy to use in a simple simulation of particle decay during fission (such as in JULIAN), where there is no change in deformation energy with time. It may be expected that ΔE_x will carry some information on this aspect of fission.

Applying this procedure to the experimental values of $\nu_{\rm pre}$ and ε_ν for the 158.8 MeV ^{18}O reactions gave values of τ_f and ΔE_x shown in Fig. 3 as a function of the compound nucleus mass number A(CN). The former are closely grouped around 40×10^{-21} s, appearing to be independent of mass (fissility). For the nuclei below A(CN)=220, ΔE_x is centered at -4 MeV. This would be consistent with neutron emission at deformations larger than equilibrium. For the heaviest system, $\Delta E_x=20$ MeV. For this reaction, the fission barrier is insignificant, and larger deformations will result in an increase in excitation energy, up to a maximum possible value of 49 MeV at scission if all energy is dissipated into heat. This change in E_x may be called the effective fission Q value, given by the masses of the compound nucleus M(CN), of the two fission fragments $[M(F_1),M(F_2)]$ and the TKE, thus

$$Q_f=M(\mathrm{CN})-[M(F_1)+M(F_2)+\mathrm{TKE}]\ .$$

Thus the increase in E_x can be interpreted as evidence for the decreasing role of the fission barrier as it becomes small and moves closer to the equilibrium configuration, and may also indicate the presence of fast fission (fission without barrier) and/or quasifission.

Referring back to Fig. 3, for the reaction of ^{18}O with ^{238}U, the measured $\nu_{\rm tot}$ was lower than that calculated, probably due to incomplete fusion resulting in a lower excitation energy of the compound nucleus. Reducing the initial E_x by 18 MeV gives good agreement in $\nu_{\rm tot}$, but reduces both $\nu_{\rm pre}$ and ε_ν. In order to regain the previous fit, ΔE_x must be increased by 18 MeV to compensate. This results in the hollow data point. Of course the value of τ_f is unchanged. The same procedure was carried out for the ^{18}O+^{197}Au data point.

From this example, it is clear that the value of ΔE_x determined depends both on the level density parameter used and on reliable calculations of $\nu_{\rm tot}$. In contrast, the value of τ_f is not subject to these uncertainties.

Turning to the 288.0 MeV ^{16}O data shown in Fig. 4, the results are quantitatively similar to those discussed above, with the average $\tau_f\sim30\times10^{-21}$ s, and ΔE_x near zero (within error) for lighter nuclei, increasing above A(CN)$\sim$210, when the effect of incomplete fusion is accounted for (hollow points). There seems to be a trend to shorter times as the fissility increases, which may be real, reflecting the increasing importance of fission without barrier (fast fission).

Within this model, which assumes total suppression of the fission probability for a fixed time, and a neutron evaporation cascade where ΔE_x does not change with time, these two sets of reactions show that the fusion-fission time scale is within the range $(35\pm15)\times10^{-21}$ s, independent of uncertainties in the level density parameter and the excitation energy after the fusion process. Remaining uncertainties lie only in the details of the neutron transmission coefficients, and in the deformation dependence of the neutron binding energy [34]. These problems will not be addressed in this paper. The values of ΔE_x for each set of reactions are consistent; the dependence on A(CN) can be explained qualitatively in terms of the decreasing importance of the fission barrier and the increase in the effective fission Q value. In reality ΔE_x will be different at the time of emission (t_i) of each neutron emitted, thus in our simple picture ΔE_x is an average over these values:

$$\Delta E_x=\frac{1}{\nu_{\rm pre}}[\Delta E_x(t_1)+\Delta E_x(t_2)+\cdots+\Delta E_x(t_\nu)]\ .$$

A more quantitative interpretation of deduced ΔE_x values will be given in Sec. V.

The use of both the mean pre-scission neutron kinetic energy and the multiplicity in deducing fission characteristics is clearly an advance on the original neutron clock concept; by extension, this may be called the neutron clock thermometer.

2. *Mass-asymmetry dependence*

For the 158.8 MeV ^{18}O data, sufficient statistics were obtained in the reactions with ^{238}U, ^{197}Au, ^{154,144}Sm to allow the extraction of neutron angular correlations for up to nine mass gates. The measured characteristics of the fragments for each mass gate were used in the neutron multiple source fitting program, neglecting recoil effects. This has been shown [29] to cause no appreciable error.

The neutron multiplicities for these reactions are given in Tables VII to X, derived using the pre-equilibrium source characteristics determined for the full mass distribution. The multiplicities for ^{18}O+^{197}Au and ^{18}O+^{154}Sm are shown in Fig. 7, together with a contour plot of the singles fission yields, showing the mass gates applied and the TKE according to the Viola systematics as calculated using the denominator of Eq. (1). Several features are of note. The post-scission multiplicities from fragment 2 (hollow triangles) have been plotted not at the mass of fragment 1 (hollow squares), but at their actual masses [$A_2=A(\mathrm{CN})-A_1$] in our approximation). The fact that there is a very small systematic difference most likely represents an error in the mass calibration of $\sim$2%, or less likely, a discrepancy in the relative neutron detector efficiencies of $\sim$5% between those sensitive to $\nu_{\rm post_1}$ and to $\nu_{\rm post_2}$, respectively. The multiplicity within

TABLE VII. Mass-split dependence of neutron multiplicities for the reaction 158.8 MeV $^{18}O+^{238}U$. The mean fragment mass A_1 observed at laboratory angle Θ_1 is associated with post-scission neutron multiplicity ν_{post_1}, while ν_{post_2} is associated with the complementary fragment of mass $A_2 = A(CN) - A_1$. The mean pre-scission neutron kinetic energy is given by ε_ν, in MeV.

A_1	78	104	120	130	140	158	182
ν_{pre}	1.35	3.95	4.80	4.90	5.00	4.20	3.60
(error)	(1.25)	(0.30)	(0.50)	(0.50)	(0.60)	(0.30)	(1.20)
ε_ν	2.8	3.25	3.35	3.25	3.12	3.18	
(error)	(1.2)	(0.20)	(0.15)	(0.20)	(0.15)	(0.20)	
ν_{post_1}	2.35	3.05	3.70	4.35	4.80	5.40	6.20
(error)	(0.35)	(0.20)	(0.30)	(0.35)	(0.25)	(0.30)	(1.15)
ν_{post_2}	6.90	5.25	4.55	4.25	3.65	3.10	2.10
(error)	(0.60)	(0.25)	(0.25)	(0.30)	(0.20)	(0.10)	(0.30)
ν_{tot}	10.60	12.25	13.05	13.50	13.45	12.70	11.90
(error)	(0.30)	(0.20)	(0.30)	(0.25)	(0.20)	(0.20)	(0.15)

TABLE VIII. Mass-split dependence of neutron multiplicities for the reaction 158.8 MeV $^{18}O+^{197}Au$. Symbol meanings are as described for Table VII.

A_1	69	81	90	100	110	120	130	140	151
ν_{pre}	2.40	3.35	3.45	3.90	4.00	4.00	3.85	3.45	2.90
(error)	(0.70)	(0.45)	(0.22)	(0.18)	(0.20)	(0.30)	(0.30)	(0.35)	(1.00)
ε_ν	3.16	3.19	3.31	3.34	3.45	3.34	3.32	3.19	3.18
(error)	(0.50)	(0.23)	(0.17)	(0.15)	(0.12)	(0.11)	(0.13)	(0.27)	(0.69)
ν_{post_1}	1.35	1.65	2.20	2.50	2.85	3.10	3.70	3.90	4.50
(error)	(0.25)	(0.22)	(0.18)	(0.15)	(0.20)	(0.20)	(0.25)	(0.25)	(1.00)
ν_{post_2}	4.70	4.20	3.60	3.10	2.75	2.50	2.00	1.60	1.30
(error)	(0.50)	(0.30)	(0.20)	(0.15)	(0.15)	(0.15)	(0.18)	(0.20)	(0.25)
ν_{tot}	8.45	9.20	9.25	9.50	9.60	9.60	9.55	8.95	8.70
(error)	(0.30)	(0.25)	(0.20)	(0.18)	(0.20)	(0.20)	(0.20)	(0.25)	(0.35)

TABLE IX. Mass-split dependence of neutron multiplicities for the reaction 158.8 MeV $^{18}O+^{154}Sm$. Symbol meanings are as described for Table VII.

A_1	52	61	71	80	90	100	110	119
ν_{pre}	2.30	3.35	4.05	4.00	4.30	3.90	3.50	2.80
(error)	(0.70)	(0.30)	(0.30)	(0.30)	(0.25)	(0.40)	(0.37)	(0.90)
ε_ν	3.58	3.42	3.53	3.45	3.45	3.53	3.45	
(error)	(0.88)	(0.21)	(0.16)	(0.10)	(0.10)	(0.16)	(0.26)	
ν_{post_1}	0.75	1.20	1.37	1.72	2.20	2.65	2.90	3.30
(error)	(0.30)	(0.20)	(0.20)	(0.15)	(0.15)	(0.30)	(0.40)	(1.00)
ν_{post_2}	3.50	3.00	2.75	2.60	1.85	1.70	1.40	1.30
(error)	(0.80)	(0.35)	(0.18)	(0.20)	(0.15)	(0.18)	(0.17)	(0.30)
ν_{tot}	6.50	7.55	8.20	8.30	8.35	8.20	7.85	7.45
(error)	(0.45)	(0.30)	(0.20)	(0.15)	(0.15)	(0.20)	(0.27)	(0.42)

TABLE X. Mass-split dependence of neutron multiplicities for the reaction 158.8 MeV $^{18}O+^{144}Sm$. Symbol meanings are as described for Table VII.

A_1	50	60	70	80	90	100	110
ν_{pre}	1.25	2.10	2.25	2.60	2.40	2.00	1.75
(error)	(0.30)	(0.20)	(0.20)	(0.20)	(0.20)	(0.35)	(0.60)
ε_ν	3.36	3.50	3.53	3.61	3.60	3.45	2.92
(error)	(0.55)	(0.35)	(0.17)	(0.15)	(0.18)	(0.25)	(0.80)
ν_{post_1}	0.85	1.05	1.30	1.50	2.00	2.65	2.85
(error)	(0.10)	(0.15)	(0.10)	(0.15)	(0.20)	(0.20)	(0.60)
ν_{post_2}	3.25	2.85	2.30	1.70	1.55	1.30	1.10
(error)	(0.25)	(0.20)	(0.15)	(0.15)	(0.10)	(0.15)	(0.20)
ν_{tot}	5.35	6.00	5.85	5.80	5.95	5.95	5.70
(error)	(0.50)	(0.25)	(0.20)	(0.20)	(0.15)	(0.20)	(0.40)

error increases linearly with fragment mass. This is a reflection of the perhaps surprising dependence of ν_{pre} on mass split. Indeed, comparing the variation of ν_{pre} and ν_{tot} with mass, the variation of ν_{pre} is at least as large as that of ν_{tot}. The variation of the latter is simply a Q value or energy balance effect, so the question is raised whether this is also the explanation for the ν_{pre} results.

Three effects seem likely to contribute to the observed variation in ν_{pre}. If we assume that in order to observe a given mass asymmetry, the system passed over the relevant conditional saddle point (which is of course higher than for a symmetric split) then a phase-space argument may be applied. At any given time, an ensemble of nuclei will have a distribution of excitation energies due to the random nature of decay, and those with the highest energy (smallest ν_{pre}) will be more likely to pass over the higher conditional barriers. The second effect is due to the fact that the system may possibly spend an ap-

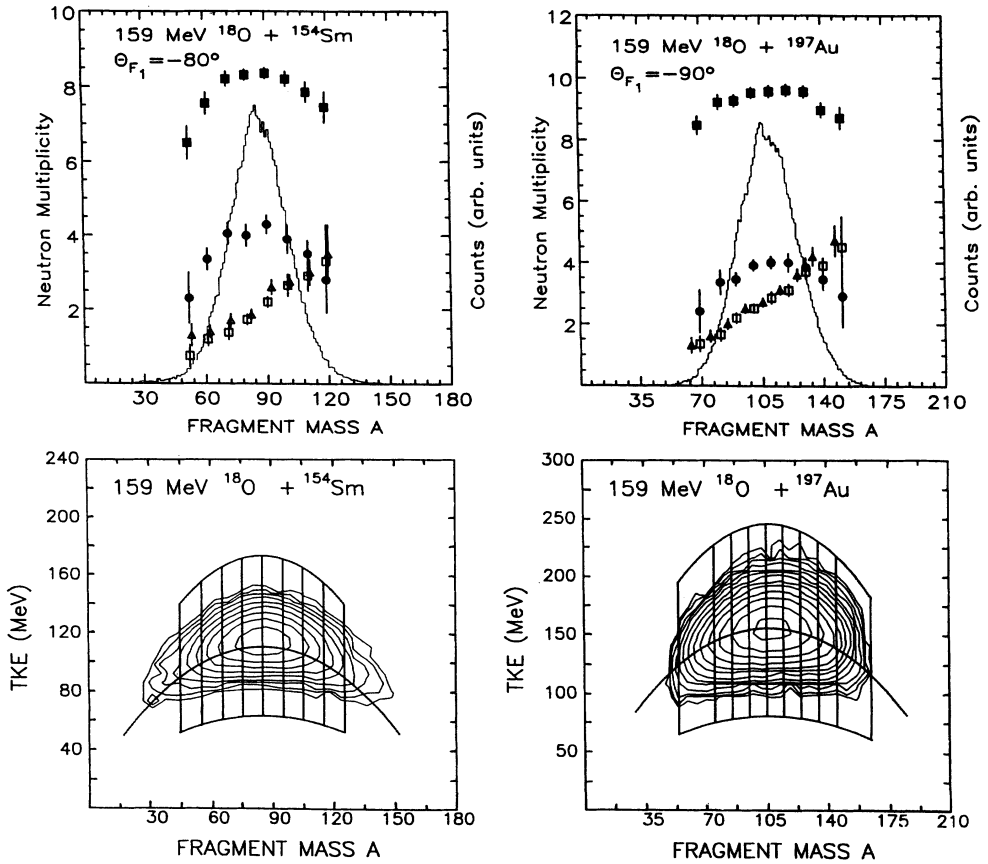

FIG. 7. The lower panels show the singles fission yield in terms of the observed fragment mass and TKE, which were determined assuming no evaporated particles (see text). Contour lines represent a factor 2 change in yield. The curved line shows the calculated TKE according to the Viola systematics. Vertical lines show the mass gates applied. The upper panels show the projected mass distribution, and the neutron multiplicities, ν_{pre} (filled circles), ν_{tot} (filled squares), and ν_{post_1}, ν_{post_2} (outlined squares and triangles, respectively).

preciable part of τ_f close to its final mass asymmetry, either near the (higher) barrier or between the saddle configuration and the scission configuration, also higher in energy for asymmetric splits. Thus such nuclei will have less thermal energy, and will emit fewer neutrons in a given time. These two effects would tend to reduce ε_ν for asymmetric splits. The third and most interesting possibility is simply that the fission time scale τ_f is indeed shorter for asymmetric mass splits. If this were the only effect, ε_ν should be higher for asymmetric splits. The experimental data show that ε_ν is within error independent of mass split (see Tables VII to X), which could be interpreted to support a combination of effects. A quantitative analysis based on these effects is in preparation.

For the 288 MeV ^{16}O-induced data, the variation of ν_{pre} with mass asymmetry could only be extracted from the reactions on ^{197}Au and ^{109}Ag. In the latter case, due to the high excitation energy and low mass of the system, there was a considerable broadening of the fragment-fragment correlation due to evaporation. This made it difficult to apply gates to the data which did not result in cuts in the angular range of the fragment due to the acceptance of the large MWPC. Such cuts would perturb the angular correlation of neutrons, and must be avoided. By applying gates with limited acceptance in TKE, symmetric about the peak [see Fig. 9(a)], such effects were minimized, but not totally eliminated, resulting in greater uncertainty in multiplicities for this projectile-target combination. Such problems were not present in the reaction with ^{197}Au.

The neutron multiplicities for these reactions are given in Tables XI and XII; for the ^{197}Au target, the pre-equilibrium multiplicity was fitted for each mass bin. It is notable that for the ^{109}Ag target, it was found that there was an out-of-plane anisotropy in the pre-scission yield, sufficient to reduce the multiplicity by $\sim 20\%$ compared to assuming isotropic emission. This is presumably related to the very high rotational frequency required to make the compound nucleus undergo fission. This is a subject for further experimental study. The experimental data for the ^{197}Au target are shown in Fig. 8, together with the mass-TKE contour diagram of the fission yield and the gates applied. The variation of all components

TABLE XI. Mass-split dependence of neutron multiplicities for the reaction 288.0 MeV ^{16}O+^{197}Au. Symbol meanings are as described for Table VII.

A_1	60	80	100	120	140
ν_{pre}	4.6	5.9	6.3	6.55	6.2
(error)	(1.0)	(0.5)	(0.4)	(0.4)	(0.6)
ε_ν	4.16	4.47	4.52	4.45	4.39
(error)	(0.58)	(0.28)	(0.20)	(0.27)	(0.35)
ν_{post_1}	1.4	2.05	2.90	3.75	4.50
(error)	(0.4)	(0.3)	(0.3)	(0.3)	(0.6)
ν_{post_2}	5.9	4.8	3.6	2.9	2.1
(error)	(1.0)	(0.5)	(0.3)	(0.3)	(0.4)
ν_{tot}	11.9	12.8	12.8	13.2	12.8
(error)	(0.6)	(0.3)	(0.3)	(0.3)	(0.5)

with mass is essentially identical to that seen at the lower bombarding energy, the only difference being that ν_{pre} is raised by 2.5 to 3 neutrons. This similarity is emphasized by the inclusion of the ν_{pre} results for that reaction, indicated by the stars. This result is consistent with the picture [26] that due to decreasing neutron lifetimes, increased excitation energy is removed before large-scale collective motion occurs, and the information on dynamics is contained in the last neutrons emitted, not the first.

The experimental data for the reaction on the ^{109}Ag target are shown in Figs. 9(a) and (b), in the familiar format. Considerable time was taken to collect a large number of the rare fission-neutron coincidences from this reaction. The reason was that the compound nucleus ^{125}Cs is near the Businaro-Gallone point [44,45], and so the variation with mass asymmetry of the heights of the conditional (mass asymmetry constrained) saddle points is very small. This leads to a fission mass distribution which is not strongly peaked at symmetry, but is rather flat, or even peaked at asymmetric mass splits. The projected mass yield for the TKE cut shown in the figure proves that there is indeed little variation of fission barrier height with mass asymmetry. The effect of this is to essentially eliminate the phase-space arguments (made in the case of a symmetric fission yield) which would lead to

TABLE XII. Mass-split dependence of neutron multiplicities for the reaction 288.0 MeV ^{16}O+^{109}Ag. Symbol meanings are as described for Table VII.

A_1	22	30	40	50	60	70	80
ν_{pre}	2.4	3.2	4.2	4.1	4.0	4.55	3.2
(error)	(1.2)	(1.2)	(0.8)	(0.8)	(0.5)	(0.8)	(1.0)
ε_ν	4.5	4.7	4.75	5.05	5.15	4.8	5.0
(error)	(1.1)	(0.3)	(0.4)	(0.4)	(0.4)	(0.4)	(0.5)
ν_{post_1}	0.4	0.55	0.35	0.65	0.95	0.90	1.50
(error)	(0.25)	(0.30)	(0.25)	(0.30)	(0.50)	(0.40)	(0.50)
ν_{post_2}	2.0	1.9	1.3	1.3	1.3	1.0	1.0
(error)	(0.8)	(0.8)	(0.7)	(0.5)	(0.5)	(0.5)	(0.4)
ν_{tot}	4.8	5.65	5.85	6.05	6.25	6.45	5.7
(error)	(0.4)	(0.4)	(0.3)	(0.3)	(0.3)	(0.35)	(0.3)

the expectation of a reduction in ν_{pre} for asymmetric splits. This leaves only the effect of a reduction in the dynamical time scale for asymmetric fission. The experimental data do show a reduction in ν_{pre} for large asymmetry. This is illustrated more clearly in Fig. 9(c), where ν_{pre} is plotted as a function of the mass of the light fragment. Experimental evidence [46] from mass yields of similar systems suggests that there is no unique boundary between fission and evaporation. Extending this idea to its limit, it is clear that for a light fragment of mass number one, charge zero, ν_{pre} is zero by definition, and the dynamical time scale is very short ($\sim 10^{-22}$ s). The problem of converting the measured ν_{pre} and ε_ν into a time scale is complicated in this case by the multiplicity of $Z=1$ and $Z=2$ particles of ~ 1 each. Since these are not measured, one must rely on the statistical model code to model the widths correctly. Another problem may be the variation of mass yield with angular momentum [47] introducing a correlation between charged particle competition and mass asymmetry which is not accounted for. A third problem is the possibility of contamination by deep inelastic products.

Bearing in mind these problems in interpreting the data for 288 MeV $^{16}O+^{109}Ag$, the results of an analysis of the ν_{pre} and ε_ν data as a function of the mass of the light fragment are shown in Fig. 9(d). There is a strong dependence of τ_f on the mass asymmetry. For the reaction of ^{18}O with ^{nat}Ag at a bombarding energy of 1512 MeV, the delay time between emission of intermediate mass fragments (IMF), or before IMF emission, for fragments of mean mass around 20 was determined by the Coulomb correlation method or from the multiplicity distributions [48] respectively, to be between 250 and 500 fm/c, or $(0.8-1.7)\times 10^{-21}$ s. These points are shown by the hollow triangles. Considering the uncertainties in both methods, the agreement of the points is gratifying, and gives additional weight to the hypothesis that fission and evaporation are the extremes of a unified binary decay mechanism [47], whose different characteristics are due to the different time scales associted with the emission/fission process.

This exciting result should prompt further such measurements, in particular including the charged-particle decay channels.

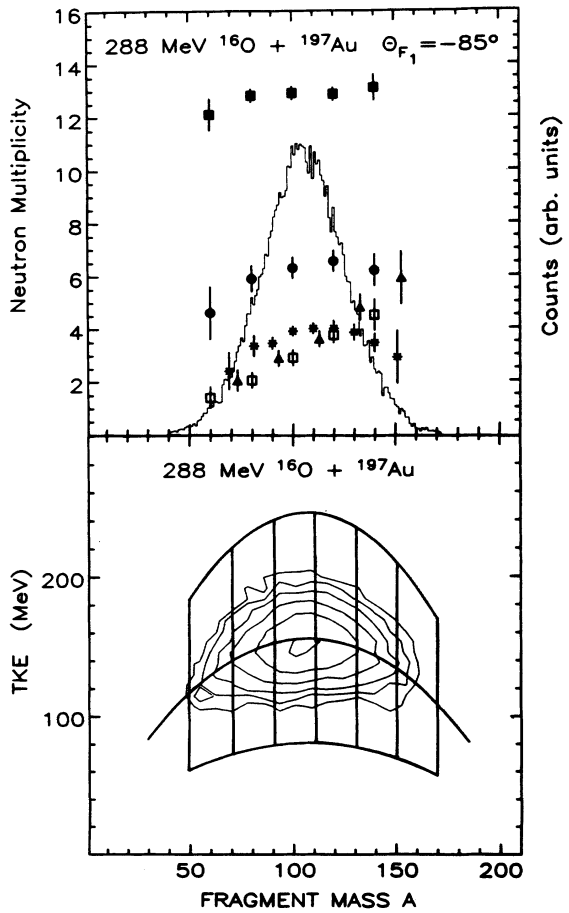

FIG. 8. As Fig. 7, but for 288.0 MeV $^{16}O+^{197}Au$. The stars show the variation of ν_{pre} for the 158.8 MeV ^{18}O-induced reaction. The ν_{pre} data for ^{16}O appear to be shifted up uniformly from these values.

3. *TKE dependence*

For the 158.8 MeV ^{18}O-induced reactions, TKE gates were applied for the reactions with ^{197}Au and ^{154}Sm. As already explained, they were applied as linear cuts in RTKE to maintain the same mass spectrum in each gate. Their appearance in the mass-TKE matrix is shown in Fig. 10. RTKE cuts were also applied to the data for 288 MeV $^{16}O+^{197}Au$. As in the case of the mass cuts, initially recoil effects due to the post-scission neutrons were neglected. For each reaction, the same phenomenon was observed, which had previously been noted [26,27], namely, that ν_{pre} showed a strong gradient, increasing with increasing TKE. The present $^{16,18}O+^{197}Au$ ν_{pre} data, those for $^{36}Ar+^{169}Tm$ [27] and those for $^{40}Ar+^{165}Ho$ [26], which will also be described later, all form compound nuclei with $Z=85$ or 87. A compilation of these recoil-uncorrected values of ν_{pre} has been made, and is shown in Fig. 11. Although each reaction results in a different E_x(CN), the absolute change in ν_{pre} as the TKE changes is similar. The lack of a physical mechanism for this effect led us to question the neglect of the recoil effect due to the detection of post-scission neutrons. Detection of such a neutron, for instance on axis with the fragment which emitted it, will result in the observation of a lower TKE. The coincident neutron yield is divided by the singles fission yield in the same RTKE gate, but detection of a post-scission neutron leads to division by the wrong singles fission counts. This effect was corrected for in the multiple-source-fitting program, and reduces the variation of ν_{pre} with TKE very substantially, but not completely as shown by the solid circles in Fig. 10. The second effect of the recoil imparted by the neutron is to change the source velocity in the fitting procedure, however, this effect causes only a small change in ν_{pre}, typically $\lesssim 0.1$ neutron. The fact that the gradient is not eliminated may reflect a physical effect; however, the fact that fitting computer-generated data, for the reaction $^{36}Ar+^{169}Tm$, with no initial dependence on ν_{pre} on TKE still leaves a gradient when the recoil effect is included [27] makes an explanation based on the fission process itself rather unlikely. Assuming that there are

still uncorrected kinematic effects, the change in ν_{pre} at each point has been increased by 40% (this results in no gradient in the fit to the computer-generated data), and gives a dependence of ν_{pre} on TKE shown by crosses in Fig. 10. Clearly, further detailed investigation of the fitting procedure is required before this effect can be conclusively explained.

B. ^{40}Ar-induced reactions

The data for reactions of ^{40}Ar on ^{238}U, ^{208}Pb, ^{197}Au, ^{181}Ta, ^{165}Ho, and ^{141}Pr will be presented in the same order as the ^{16,18}O-induced reactions. A neutron angular correlation for symmetric fission of ^{40}Ar+^{238}U is shown in Fig. 12, and illustrates the high quality of data obtained.

1. All fissions

For the reactions with ^{238}U and ^{208}Pb, the mass distributions were very wide, extending almost to the projectile and target masses, so in presenting multiplicities, those corresponding to a mass cut around symmetric fission will be given. Properties of the fission fragments and the neutron multiplicities are given in Table XIII. Figure 13 shows the measured values of ν_{pre} and ν_{tot} as a function of A(CN). The pre-scission multiplicity rises up to A(CN)=221 (Ta target), then falls, but again rises for the ^{238}U target [A(CN)=278]. Values of ν_{tot} increase monotonically, due to Q values. (Here ν_{pee}, typically 0.4, is included in ν_{tot}.)

The fusion cross sections were determined by extrapolation from the wealth of experimental data existing for ^{40}Ar fusion reactions [49]. In making calculations with JULIAN, Viola TKE values were used, and the full excitation energy for complete fusion was taken, level density parameters being based on the equations of Ref. [43]. Total neutron multiplicities so calculated are shown in Fig. 13 as hollow points, which are in excellent agreement with the measurement.

The measured ν_{pre} and ε_ν values were fitted by adjusting τ_f and ΔE_x, as previously described for the ^{16,18}O data, and the results are shown in the right panels of Fig. 13. Times very similar to those determined for the ^{16,18}O-induced fission can be seen, $\sim 40\times 10^{-21}$ s, while the trend in ΔE_x is also similar. These results will be discussed in more detail in Sec. V, but it is notable that, for the reactions where quasifission is not expected to be dominant [i.e., excluding ^{40}Ar+^{238}U, A(CN)=278], the agreement in both τ_f and ε_ν perhaps suggests that the fusion time (expected to be longer for more symmetric

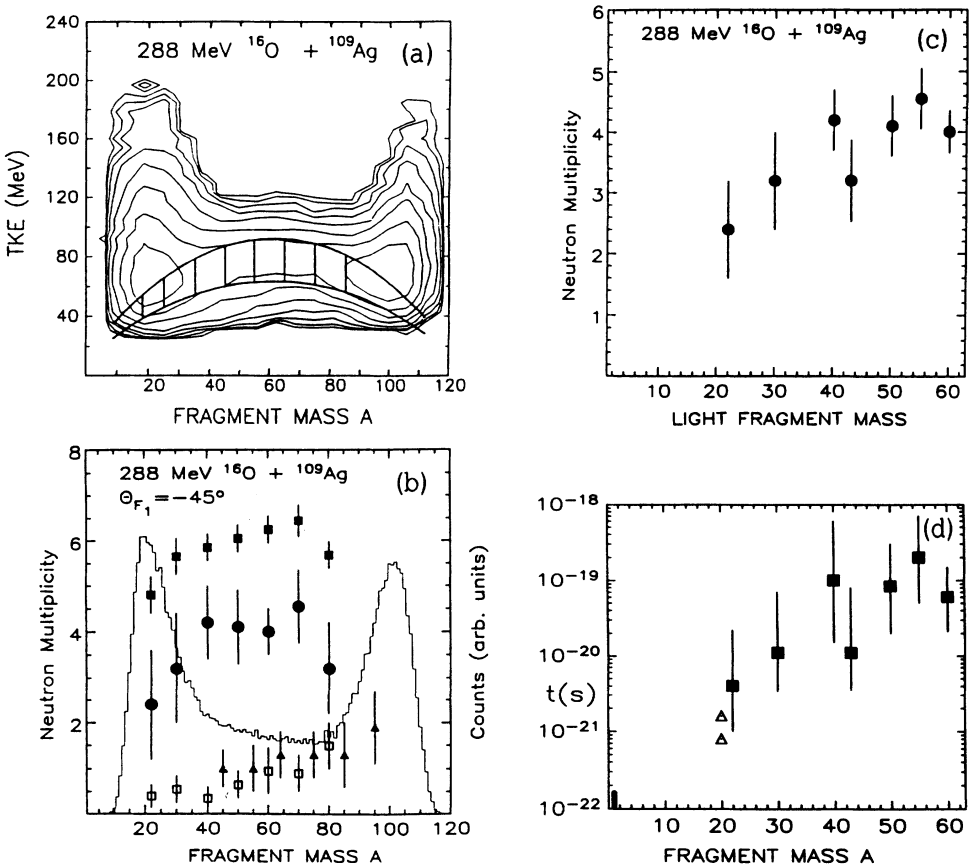

FIG. 9. Results for the reaction 288.0 MeV ^{16}O+^{109}Ag. Panel (a) shows the gates applied to the mass-TKE matrix corresponding to the data points given in panel (b), where the projected mass distribution is shown, together with the neutron multiplicities, using the same convention as in Fig. 7. Panel (c) shows ν_{pre} only, as a function of the light fragment mass, while panel (d) shows τ_f values deduced from the neutron multiplicities (filled squares), and from measurements of the fragments themselves in reactions at higher energies [48] (outlined triangles). For more details, see text.

projectile-target combinations) is not as long as the time required for fission.

2. *Mass-asymmetry dependence*

Sufficient statistics were obtained for the $^{40}Ar+^{208}Pb$, ^{238}U reactions to allow gates to be applied to the fragment mass. For the former reaction, fission fragments were detected at $-24°$, $-46°$, and for the latter, at $-24°$, $-34°$, $-46°$, $-56°$. Experimental results for the latter are given in Table XIV and the neutron multiplicities at $-24°$ and $-46°$ for each reaction are shown in Figs. 14 and 15, together with a projection of the mass yield. In both cases, the mass distribution at $-24°$ is asymmetric, slightly for the ^{208}Pb target, and grossly for the ^{238}U target. This is consistent with previous measurements [7] for similar projectiles on a ^{238}U target, and indicates that a small (^{208}Pb) or large (^{238}U) fraction of fission occurs before memory of the beam direction is lost, in other words before a half rotation of the composite nucleus. This information can be used to estimate the lifetime before scission, depending on the moment of inertia (compactness) of the composite system. From the data of Ref. [7], a time of $\lesssim 10\times10^{-21}$ s may be expected for the reaction

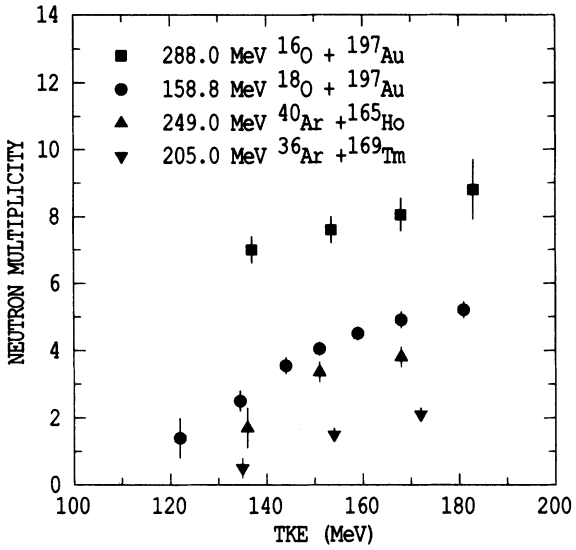

FIG. 11. Variation of the pre-scission neutron multiplicity with TKE for reactions leading to compound nuclei with $Z=85$ or 87, fitted *without* taking account of corrections to the TKE of the fragments due to the observed neutron. This leads to incorrect results, giving a spurious increase in ν_{pre} with TKE [29].

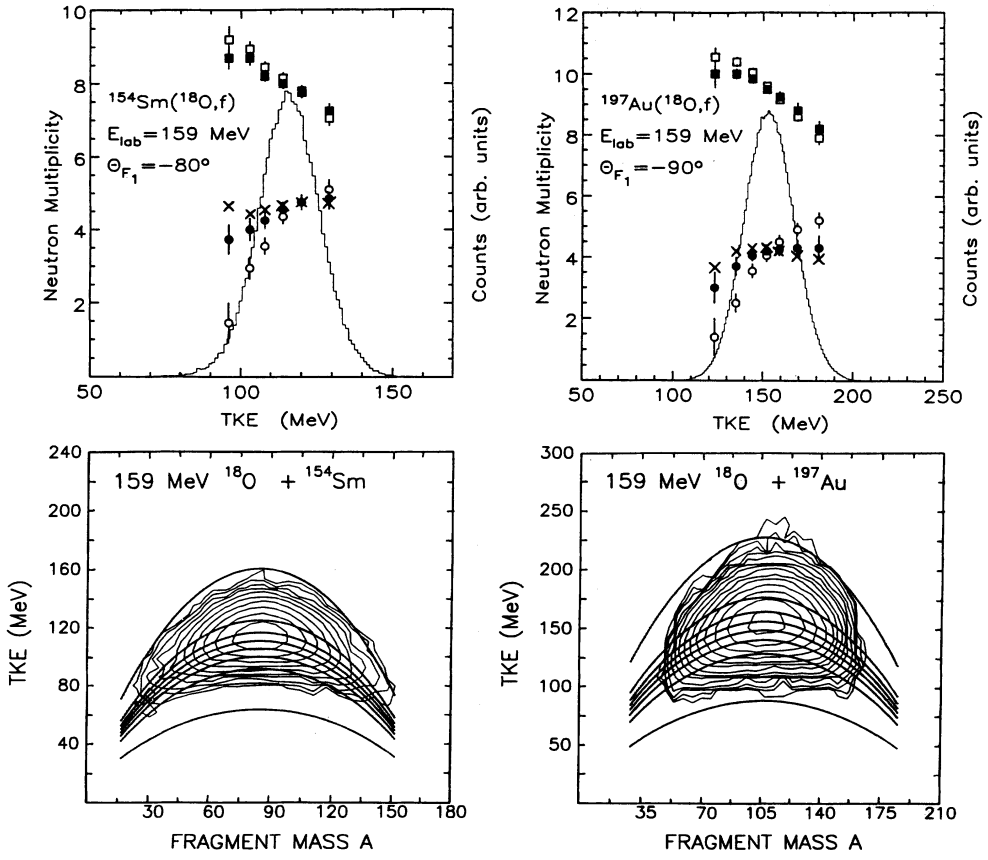

FIG. 10. The lower panels show the same data as in Fig.7, but with the linear cuts in RTKE (see text), which correspond to the curved cuts in TKE which are shown. Gates of this form result in the same mass distribution for each TKE cut, avoiding bias to the multiplicity data which would occur if each TKE cut had different mass distributions. The upper panels show the total projection of the TKE, together with the deduced pre-scission neutron multiplicities (lower points) and total multiplicities (upper points) for different fitting conditions, plotted at the mean TKE corresponding to each of the gates in mass and TKE shown below. The crosses represent the final conclusion, namely, that in fusion-fission reactions, ν_{pre} is independent of TKE.

with ^{238}U, and longer on average for the reaction with ^{208}Pb.

Turning to the neutron multiplicities in Figs. 14 and 15, within error there is no change with fission detector angle, and also no dependence on whether the heavy fragment or the light complementary fragment is detected. As has previously been discussed [26], so long as ν_{pre} reflects the pre-scission time, this last observation suggests that the correlation of mass split with reaction time is not strong, supporting the suggestion that the correlation which might initially be expected [7] is almost lost due to strong fluctuations independently in both reaction time and mass split [13].

Having observed that for a given fragment mass, ν_{pre} is within error independent of the detection angle, it is also of interest to apply the analysis of both ν_{pre} and ε_ν to all the ^{40}Ar+^{238}U data. Values of τ_f and ΔE_x so determined are shown in Fig. 16, grouped according to the detection angle of the fission fragments in the laboratory frame. Here the error bars shown represent relative uncertainties, which are smaller than the absolute uncertainties tabulated; this subject is discussed in Sec. IV A 1. These results show some very interesting features. First, τ_f is within error independent of mass split at any given angle. ΔE_x shows a strong dependence on mass split, reflecting the variation of Q_f (shown by the dashed curves). The average value of τ_f increases with angle, while the average value of ΔE_x decreases. These trends have been summarized in the right-most panels, where τ_f is shown as a function of center-of-mass angle for each data point in the lower panel, while the difference between ΔE_x and Q_f is shown versus the center-of-mass angle in the upper panel. We believe that these data may be interpreted as follows. Suppose that in the collisions of the two nuclei, the composite nuclei (mononuclei) are formed at various elongations, due to fluctuations and/or

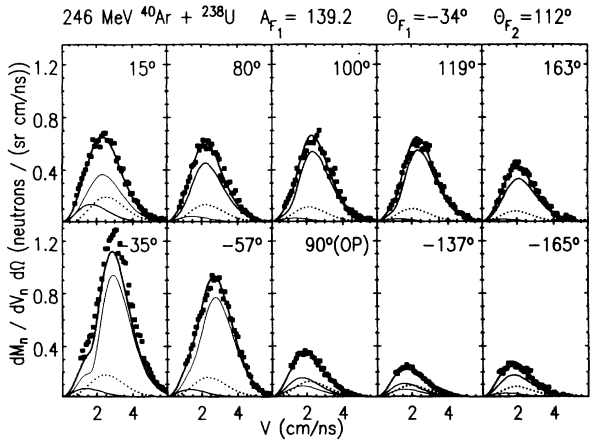

FIG. 12. Measured neutron velocity spectra for a symmetric mass split, for the reaction and the angles indicated. The components of the fit comprise pre-scission (dotted lines), post-scission from fragment 1 (thin lines), and post-scission from fragment 2 (thick lines). The total (indicated by the upper curves) is a good representation of the data except for the −35° data, which was not included in the fit due to a possible normalization error. The peaking of the post-scission neutron yield in the direction of the fragments (Θ_{F1} and Θ_{F2}) is clear.

TABLE XIII. Neutron multiplicities and statistical model input parameters for the reactions of 249.0 MeV ^{40}Ar.

Target	A(CN)	$\frac{A(\mathrm{CN})}{a_\nu}$	σ_{fus} (mb)	l_{fus}	E_x(CN)[a] (MeV)	ν_{pre}[b] (error)	ν_{pre} (error)	ε_ν (MeV) (error)	ν_{post} (error)	ν_{tot} (error)	Mass-range[c]	σ_A
^{238}U	278	9.06	450	69	74.5	0.3 (0.2)	3.25 (0.20)	3.15 (0.10)	5.75 (0.25)	14.75 (0.25)	100–175	
^{208}Pb	248	8.94	600	78	74.3	0.3 (0.2)	2.00 (0.15)	3.01 (0.16)	4.45 (0.20)	10.90 (0.20)	94–154	30
^{197}Au	237	8.88	700	84	83.0	0.4 (0.2)	2.95 (0.30)	3.25 (0.20)	3.15 (0.20)	9.25 (0.20)	All	28
^{181}Ta	221	8.79	900	94	95.7	0.3 (0.2)	3.68 (0.28)	3.34 (0.14)	2.50 (0.15)	8.68 (0.20)	All	23
^{169}Tm	209	8.73	1050	100	101.2	0.3 (0.2)	3.00 (0.30)	3.34 (0.30)	2.90 (0.20)	8.80 (0.30)	All	22.5
^{165}Ho	205	8.70	1100	102	105.6	0.4 (0.2)	2.85 (0.30)	3.37 (0.20)	3.00 (0.20)	8.85 (0.20)	All	22
^{141}Pr	181	8.56	1200	103	108.8	0.3 (0.2)	2.65 (0.30)	3.58 (0.20)	1.90 (0.20)	6.45 (0.20)	All	

[a]Excitation energy above the liquid-drop ground state, without subtracting the calculated energy removed by pre-equilibrium neutrons and protons.
[b]Pre-equilibrium neutron multiplicity, for an effective temperature in the fitting program of 3.5 MeV (see text).
[c]Mass cut applied to the fission fragments for the results tabulated.

different radial velocities at contact resulting from the range of angular momenta involved. Those formed in the most compact configuration will presumably have the longest pre-scission time, and will also feel the smallest effect of Q_f, while those formed at an elongation close to that of scission will have the shortest lifetimes and will feel practically the full effect of Q_f. Because of the short pre-scission time of the latter, they will be observed at angles close to the beam, whereas the former will be distributed more evenly over a wide angular range. Thus at angles close to 90° in the center-of-mass frame, fission from the long-lived composite nuclei will be observed, whereas at forward angles there will be observed a mixture of short- and long-lived. It must be noted that the arbitrary reduction of all ν_{pre} values by one, to account for acceleration neutrons, would reduce all times by approximately a factor of 2, and it is almost certain that a correction of this order must be made. It is, however, hard to see how the trends of τ_f and ΔE_x could be explained by emission during acceleration. In order to prove or disprove this interpretation, further investigation of the effect of neutrons emitted during acceleration of the fragments (see later) and of the angular distribution of the fragments as a function of mass should be undertaken.

The larger relative errors of the $^{40}Ar+^{208}Pb$ data made the presentation of a similar analysis of dubious value, the conclusion being that within error all the data are consistent with $\tau_f \sim 20\times10^{-21}$ s and $\Delta E_x \sim 10$–20 MeV.

3. TKE dependence

The data for $^{40}Ar+^{238}U$, ^{165}Ho were analyzed as a function of TKE, using the same gates based on linear cuts in RTKE as applied to the $^{16,18}O$-induced fission. The results for $^{40}Ar+^{165}Ho$ have already been shown in Fig. 11, fitted without correcting for the post-scission neutron recoil effect. As discussed in the $^{16,18}O$ section, it seems likely that the increase in ν_{pre} with TKE is solely a spurious kinematic effect, and there is probably no dependence of ν_{pre} on TKE for these cases.

For the $^{40}Ar+^{238}U$ data, five RTKE cuts were applied to the full mass distributions at each of the four angles at which fragments were detected. Also, for the data at $\theta_F=-34°$, six RTKE cuts were applied to *each* of the five mass bins. These 50 neutron angular correlations were then decomposed, using the multiple-source-fitting program without neutron recoil corrections, into their components. In all cases, ν_{pre} increases with TKE in a similar way, and there was no apparent dependence on θ_F. The results for all masses at $\theta_F=-34°$ is shown in Fig. 17. The trend is the same as was observed in Fig. 11 for reactions leading to less-fissile compound nuclei.

C. ^{64}Ni-induced reactions

In these reactions, the mass distributions were so wide that the data can only be interpreted as a function of mass split. Fusion cross sections were estimated using evidence from three sources; the extrapolation of the few experimental measurements [7,50,51] with ^{64}Ni beams, extrapolation using the ratio of observed fissions to elastics in the ±11° monitor detectors, and calculations of an extra-push code [52]. Again, level density parameters were calculated using the formula of Ref. [43]. In the neutron spectra, there was no evidence for a pre-equilibrium source within experimental uncertainty; this is probably partly due to the low velocity of the projectile at contact, and perhaps also because of the high center-of-mass velocities, which may cause any pre-equilibrium component to be concealed in the equilibrium emission.

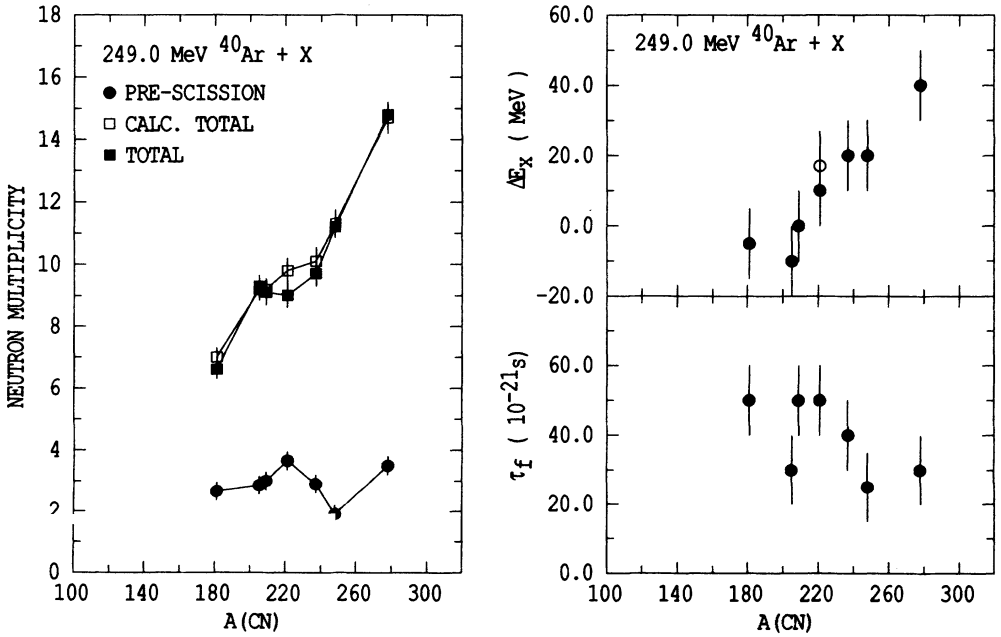

FIG. 13. The left panel shows the measured ν_{pre} and ν_{tot} values for the ^{40}Ar-induced reactions, together with the calculated ν_{tot} values. The right panel shows the deduced values of τ_f and ΔE_x, determined from the experimental ν_{pre} and ε_ν results.

1. Fragment mass yields

The contour plots of the yield of binary fragments as a function of fragment masses and TKE, shown in the lower panels of Figs. 18 and 19, reveal that the reaction mechanism in the ^{64}Ni-induced reactions is very different from those discussed previously. The mass distributions extend from below the projectile mass to above the target mass. They were so wide that the angular range of the large MWPC was insufficient, and for the heaviest fragments with lowest TKE detected in the small MWPC, the complementary fragment was not registered. This region is indicated in the figures by shading. A strong peak due to elastic scattering is present at TKE values ranging between 323 MeV (^{238}U target) and 292 MeV (^{154}Sm). System resolution generated apparent energies higher than this; each contour line corresponds to a factor of 2 change in cross section, so the relative yield above the true TKE drops very rapidly. Angular steps in the contour lines, visible for high masses, are an artifact of the contouring program. Deep-inelastic reaction products are seen, with about the same masses as the projectile and target, but TKE lower than for elastic scattering. These merge rather abruptly, but without interruption, into the quasifission events, in the same manner as observed in Refs. [7] and [51] and, as in those works, the mass yield actually has a minimum at symmetry for ^{64}Ni+^{238}U, ^{208}Pb and also for ^{197}Au. These reactions clearly belong to the category of quasifission, in which the interaction of projectile and target results in a composite nucleus (or mononucleus) which rapidly breaks apart, before full mass equilibration occurs. For the ^{64}Ni+^{238}U reaction at a slightly lower energy, it was concluded [7] that the sticking time, or reaction time was in the range 5.5×10^{-21} to 7.5×10^{-21} s. Because of the rapid breakup, it was proposed that the mononucleus never becomes more compact than the configuration of the fission saddle point, however, just how compact or extended the mononucleus is in any particular reaction has not been determined. For the ^{64}Ni+^{175}Lu, ^{154}Sm reactions, the data look qualitatively similar to the reactions on heavier targets, except for the peaking of the fragment mass yield at symmetry; this may partly be a reflection of a longer reaction time (see, however, the conclusions in the next section), possibly due to the greater energy above the Coulomb barrier. Alternatively, it may be related to the fission dynamics in a way not yet clear to us.

2. Mass-asymmetry dependence of neutron multiplicity

The properties of the pre-scission and post-scission neutrons were determined in the multiple-source fits to the neutron angular correlations for each mass gate applied. As for the reactions with lighter projectiles, a comparison of total multiplicities will be made, however, in this case it will be for the symmetric mass gate only. Calculations were performed using the same input conditions for JULIAN as previously described. The calculated ν_{tot} are in good agreement with the measurements, as shown in Fig. 20, even in the case of the ^{238}U target, despite the relatively poor quality of fit to the neutron data for that

TABLE XIV. Neutron multiplicities for mass cuts at different laboratory angles Θ_F, for the reaction 249.0 MeV ^{40}Ar+^{238}U.

Θ_F (deg)	−24	−24	−24	−24	−34	−34	−34	−34	−46	−46	−46	−46	−56	−56	−56	−56
A_1[a]	80	110	139	167	80	110	139	167	80	110	139	167	80	110	139	167	196
ν_{pre}	2.5	3.0	3.4	3.1	2.2	2.9	3.55	3.5	2.3	2.8	3.4	2.9	1.8	2.4	3.3	2.8	2.2
(error)	(0.5)	(0.5)	(0.5)	(0.5)	(0.4)	(0.3)	(0.3)	(0.4)	(0.5)	(0.5)	(0.4)	(0.5)	(0.8)	(0.5)	(0.3)	(0.5)	(0.6)
ε_ν	3.15	3.00	3.50	3.46	2.92	2.75	3.16	3.19	2.92	3.42	3.09	3.17	2.51	2.32	2.81	2.63	2.63
(error)	(0.2)	(0.2)	(0.2)	(0.2)	(0.2)	(0.2)	(0.2)	(0.2)	(0.3)	(0.2)	(0.2)	(0.3)	(0.3)	(0.4)	(0.3)	(0.4)	(0.5)
ν_{post_1}[b]	2.6	4.1	5.6	7.0	6.9	2.45	4.1	5.4	6.3	6.9	2.6	4.0	5.2	6.2	6.9	2.65	3.8	5.6	6.5	6.7
(error)	(0.2)	(0.2)	(0.3)	(0.4)	(0.6)	(0.2)	(0.2)	(0.2)	(0.3)	(0.3)	(0.4)	(0.3)	(0.5)	(0.5)	(0.6)	(0.3)	(0.2)	(0.3)	(0.4)	(0.5)
ν_{post_2}[c]	6.1	5.9	5.3	3.9	2.6	6.2	6.25	5.2	3.85	2.7	6.3	6.4	5.3	3.9	2.7	6.15	5.8	5.4	4.1	2.7
(error)	(0.4)	(0.4)	(0.3)	(0.3)	(0.4)	(0.4)	(0.4)	(0.2)	(0.2)	(0.2)	(0.5)	(0.5)	(0.3)	(0.3)	(0.3)	(0.5)	(0.5)	(0.3)	(0.3)	(0.3)
ν_{tot}[d]	11.2	13.0	14.3	14.0	12.2	10.9	13.3	14.2	13.6	12.2	11.2	13.2	13.9	13.0	11.4	11.2	12.7	14.3	13.4	11.6
(error)	(0.3)	(0.3)	(0.3)	(0.3)	(0.4)	(0.3)	(0.3)	(0.3)	(0.3)	(0.3)	(0.3)	(0.3)	(0.3)	(0.3)	(0.3)	(0.3)	(0.3)	(0.3)	(0.3)	(0.3)

[a]Mean fragment mass observed at laboratory angle Θ_F.
[b]Post-scission neutron multiplicity associated with mass A_1.
[c]Post-scission neutron multiplicity associated with mass $A_2 = A(\mathrm{CN}) - A_1$.
[d]Not including pre-equilibrium multiplicity of 0.3.

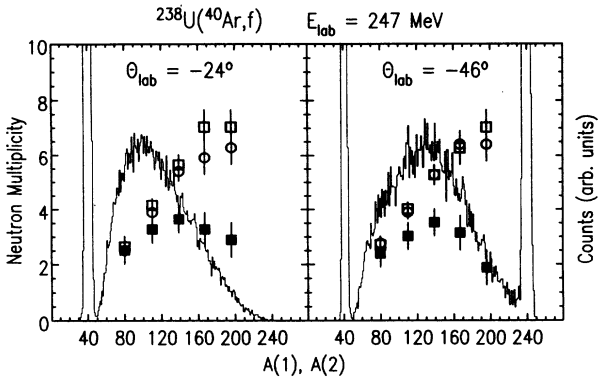

FIG. 14. Observed mass yields for the ^{40}Ar+^{238}U reaction at the laboratory angles indicated, together with the deduced values of ν_{pre}, shown by the filled squares. ν_{post_1} data are shown as a function of the mass of the fragment observed at the angle indicated [$A(1)$], and ν_{post_2} as a function of the mass of the complementary fragment [$A(2)$], by the outlined circles and outlined squares, respectively.

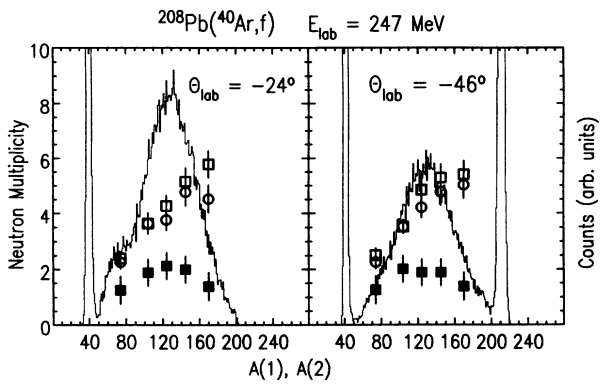

FIG. 15. As Fig. 14, but for the ^{40}Ar+^{208}Pb reaction.

reaction (discussed later). Turning to the pre-scission neutron multiplicities shown in the upper panels of Figs. 18 and 19, they show the same feature as in all previous reactions, namely, a parabolic shape peaked at symmetric mass splits. As in the explanation for the ^{40}Ar+^{238}U data, no arguments based on the probability of surmounting the fission barrier apply to these quasifission reactions, yields must be only a function of the trajectory over the potential energy surface and the reaction time. Clearly, the excitation energy is maximized for symmetric fragmentation, which is reflected in ε_ν. Applying the analysis, described previously, of ν_{pre} and ε_ν to the ^{64}Ni+^{238}U, ^{208}Pb data results in deduced values of τ_f and ΔE_x which are shown in Fig. 21. The results for the ^{64}Ni+^{208}Pb reaction can be compared directly with those for ^{40}Ar+^{238}U, since the composite system in both reactions has $Z=110$. The deduced values of both ΔE_x and τ_f are very similar to the values deduced from the ^{40}Ar-induced reaction data for fission observed at forward angles (see Fig. 16).

The most notable features in the ^{64}Ni+^{238}U results shown in Fig. 21 are the very large values of ΔE_x, up to +90 MeV, which corresponds to ~80% of the Q-value limit. Taking account of the deformation energy of the system, it seems clear that these data indicate that the neutrons are emitted close to the scission configuration. The deduced times τ_f are within error independent of fragment mass, with a mean value of $\sim 20\times 10^{-21}$ s.

Turning to the ν_{pre}, ε_ν data for the other reactions, it is clear that in some cases there is contamination of the mass cuts close to the mass of the target in particular (for instance, in the ^{64}Ni+^{175}Lu case, see Fig. 18), presumably by deep-inelastic products, resulting in low multiplicities, and poor fits to the data (due to the use in the fitting pro-

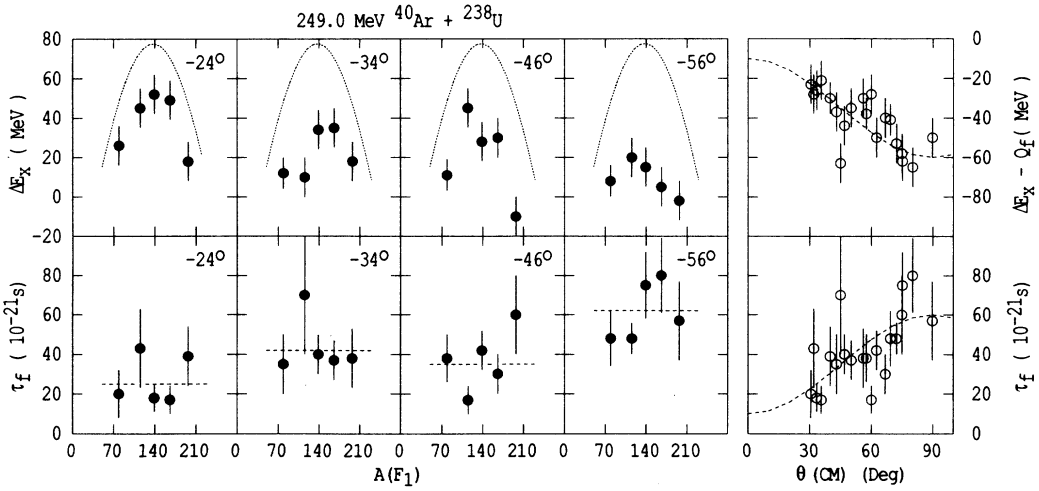

FIG. 16. Deduced values of τ_f and ΔE_x as a function of the fragment mass, each panel corresponding to the indicated mean laboratory detection angle of the fragments. Within experimental uncertainty, there is no dependence of τ_f on mass (indicated by the dashed lines), but a strong dependence on angle. The right-most panel summarizes this dependence, showing each data point at the appropriate center-of-mass angle. The dashed line guides the eye. There is, however, a strong dependence of ΔE_x on mass (upper panels), mirroring the dependence of Q_f on mass (shown by the fine dotted lines). The difference between ΔE_x and Q_f increases with angle; this is summarized in the right-most upper panel, again the dashed line guides the eye.

gram of the wrong source velocities). The remaining data points for more central mass splits cluster closely in ΔE_x and τ_f, and so can be presented as a single data point. This is done in the right-most panels of Fig. 20, where deduced values of ΔE_x and τ_f are shown averaged over the central two or three mass gates for each reaction, as a function of A(CN). The same trends are seen as previously, namely a slight decrease of τ_f with A(CN) (although the values are smaller than for the lighter projectiles) and a rapid increase in ΔE_x above $A\,(\mathrm{CN})=220$.

The values of $\tau_f \sim 20\times10^{-21}$ s are in disagreement with reaction times for symmetric splitting of the ^{64}Ni+^{238}U system deduced [7] to be $\sim 6\times10^{-21}$ s from the rotation angle of the composite system. This time is of the same order as the acceleration time of the fragments and suggests that emission during acceleration may contribute substantially to the measured ν_{pre}, and thus explains the discrepancy in reaction times noted above. If this is the case, the apparent ν_{pre} deduced from the multiple-source fit should show a strong dependence on the TKE, since a high TKE leaves little thermal energy, and results in long neutron lifetimes and a small probability of emission during acceleration. Conversely, a low

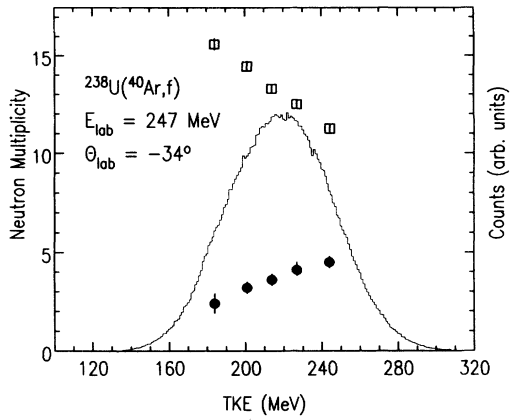

FIG. 17. Singles TKE distribution for ^{40}Ar+^{238}U. Applying cuts in RTKE, as are shown in Fig.10, allowed the TKE dependence of ν_{pre} (filled circles) and ν_{tot} (outlined squares) to be determined. No correction has been made for the effect on the fragment TKE due to the recoil imparted by the observed neutron, thus these results do not reflect the true variation of ν_{pre} with TKE. It is important to note that there is an upward gradient with TKE, as in the case of the uncorrected ^{18}O data (Fig. 10), and unlike the ^{64}Ni data (Fig. 22).

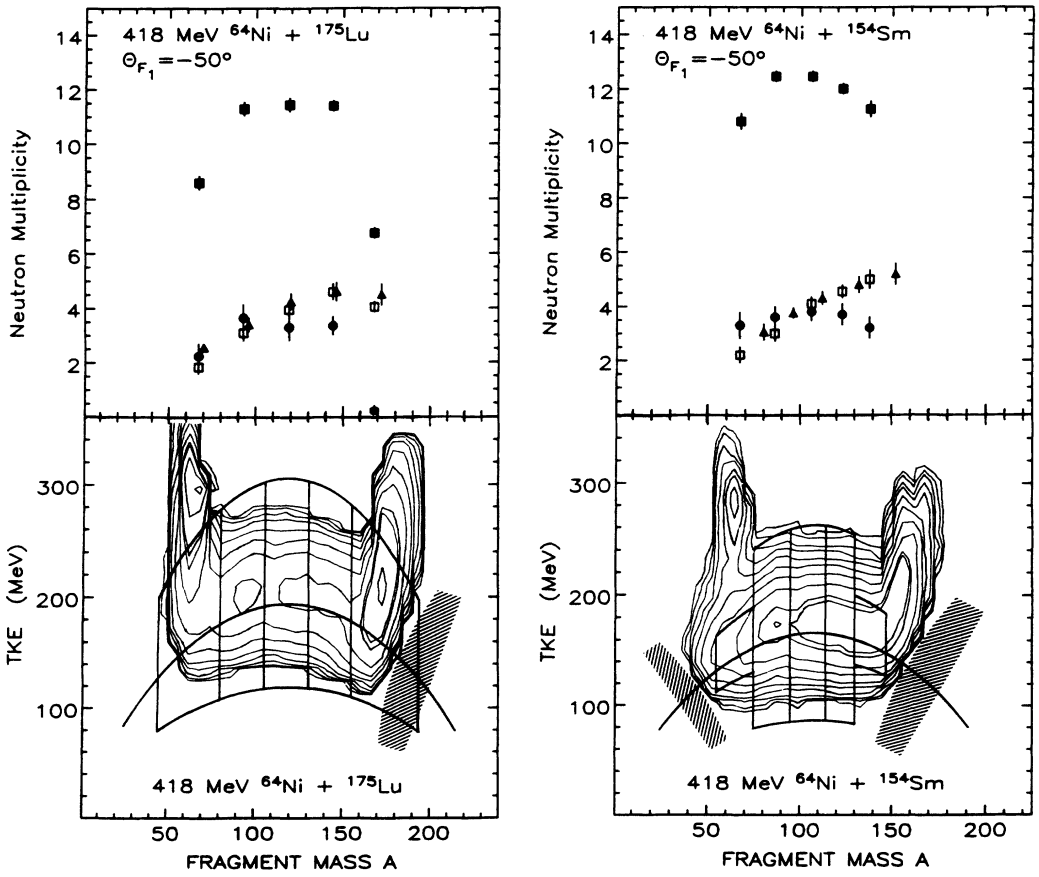

FIG. 18. The lower panels show the mass-TKE matrix for the indicated ^{64}Ni-induced reactions. Contour lines correspond to a factor of 2 change in yield. The curved line shows the mean TKE expected on the basis of the Viola systematics. The enclosed areas indicate the gates in mass and TKE applied, corresponding to the multiplicities in the upper panels, ν_{pre} (filled circles), ν_{tot} (filled squares), and ν_{post} (outlined triangles and/or squares).

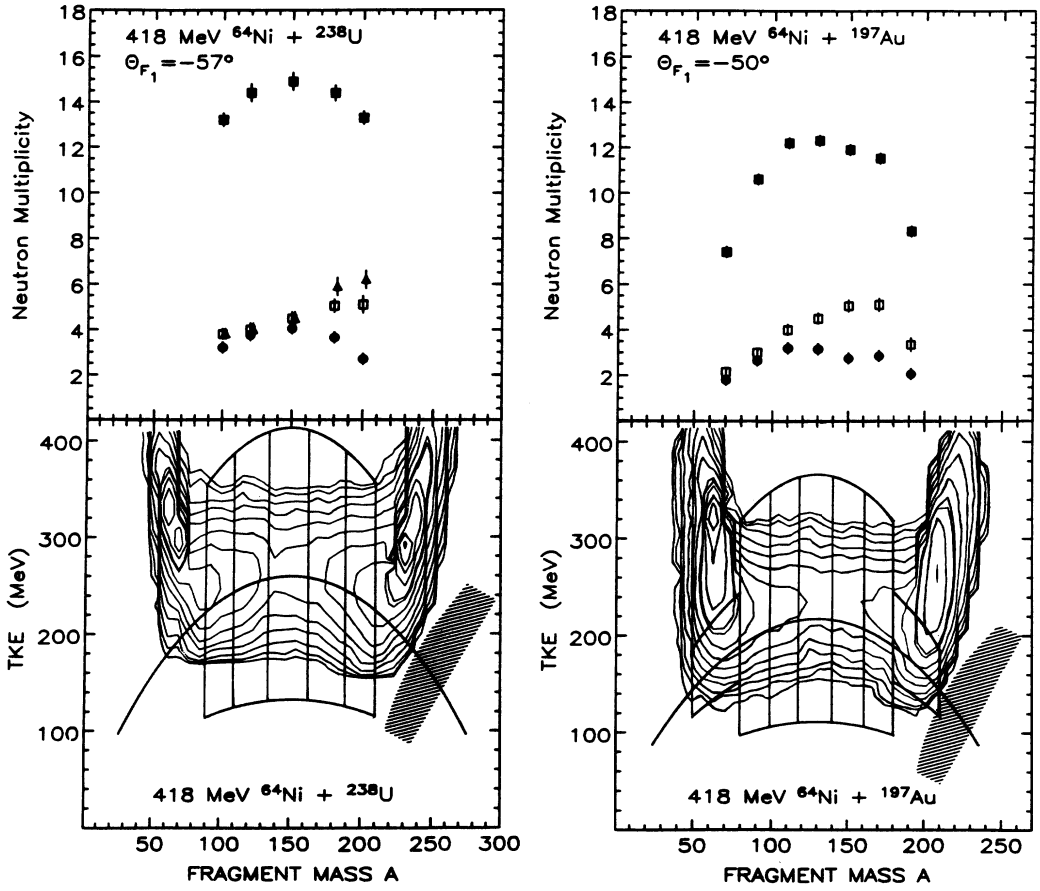

FIG. 19. As Fig. 18, for reactions on ^{238}U and ^{197}Au targets.

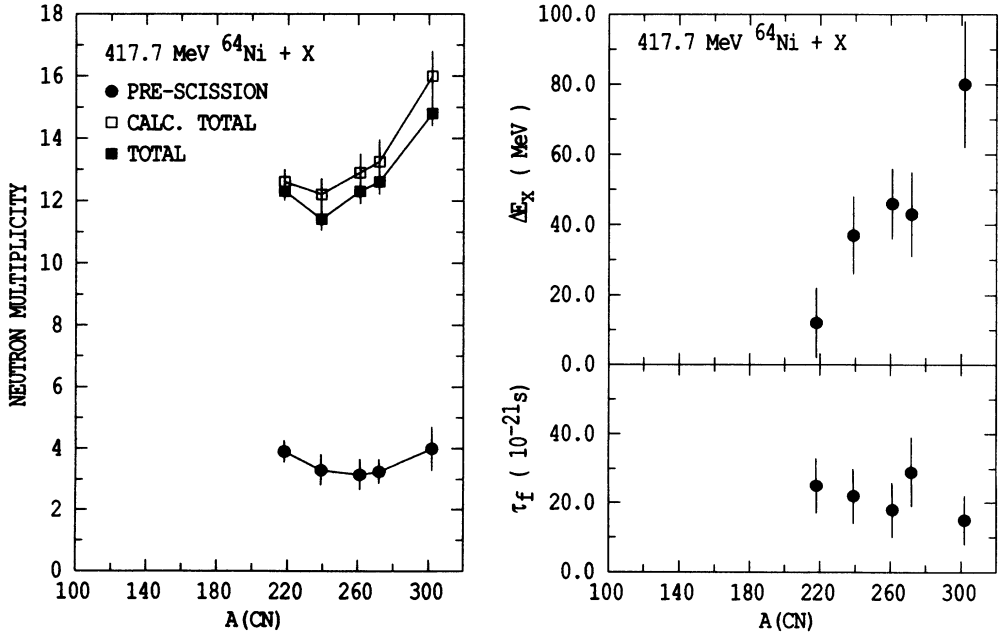

FIG. 20. The left panel shows the measured ν_{pre} and ν_{tot} values for the ^{64}Ni-induced reactions, together with the calculated ν_{tot} values discussed in the text. The right panels show the deduced values of τ_f and ΔE_x.

TKE should result in a higher deduced value of ν_{pre} than average.

3. *TKE dependence of neutron multiplicity*

Gates on RTKE were applied to a restricted range of masses around symmetry, shown in Fig. 22 for the $^{64}Ni+^{154}Sm$, ^{238}U reactions (the other reactions show similar behavior). The projected TKE distributions for these mass reactions are presented in the upper panels, and illustrate the tremendous widths of the distributions, which allow a wide range of fragment excitation energies to be sampled. The variation of ν_{pre} with TKE is shown both for fits without neutron recoil correction (hollow points) and with (solid points) as for the other reactions. The quality of fit to these data was noticeably worse than in the reactions induced by lighter projectiles, in particular for low RTKE cuts. This may be a reflection of as yet unrecognized differences in the emission patterns of the neutrons, and this possibility should be borne in mind during the following discussion of the data.

Returning to the deduced multiplicities, it is immediately obvious that the rapid decrease of ν_{pre} with TKE is

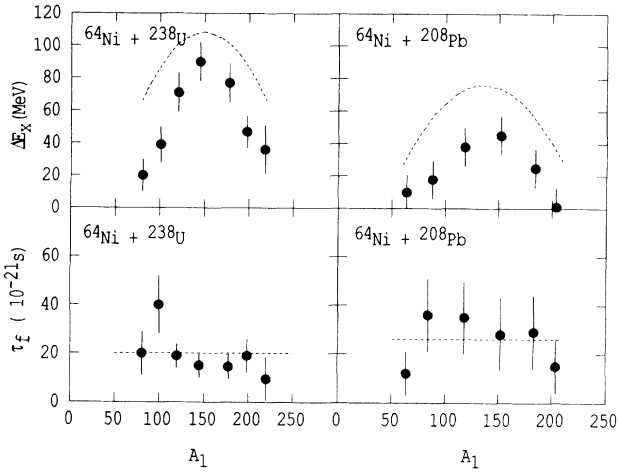

FIG. 21. The results of an analysis of the same kind as shown in Fig.16, but for ^{64}Ni-induced reactions, measured at one angle only. The same features are apparent, namely, little or no dependence of τ_f on fragment mass, but a strong dependence of ΔE_x on mass, mirroring the dependence of Q_f with mass (shown by the dashed lines in the upper panels).

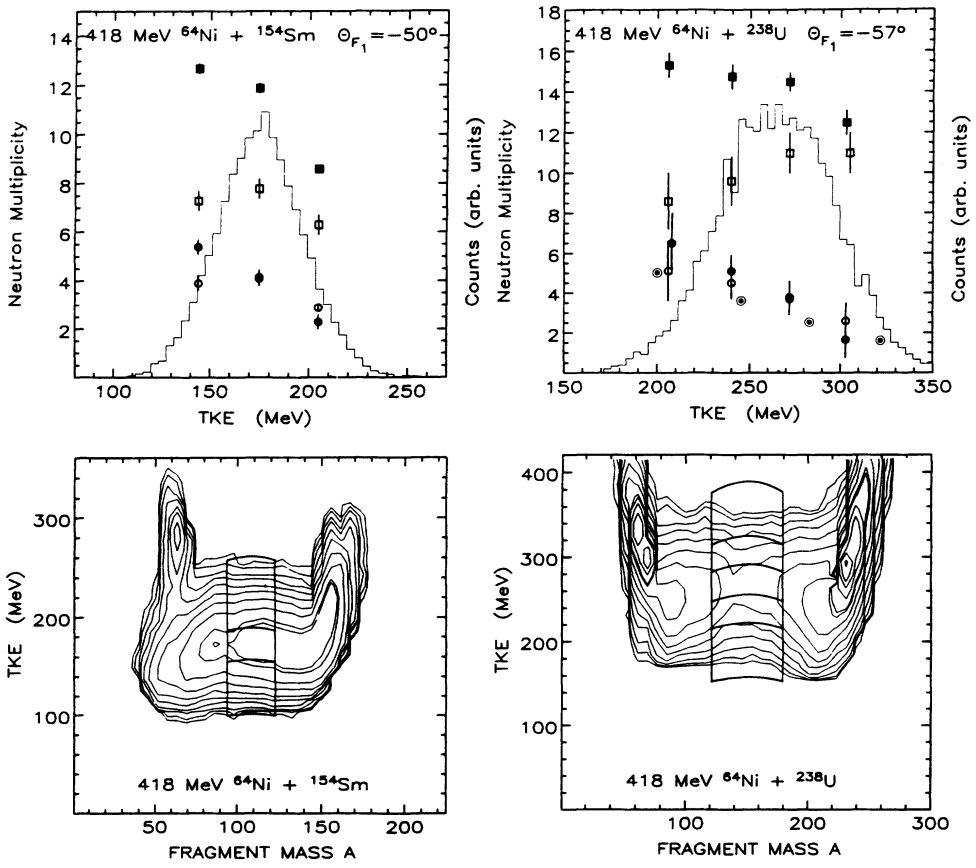

FIG. 22. The lower panels show the cuts in mass and TKE applied in order to obtain the neutron angular correlations as a function of TKE. The upper panels show the projected TKE distribution for the mass range indicated below, together with the prescission neutron multiplicities obtained with and without applying the main neutron recoil correction (filled and outlined circles), the post-scission multiplicities from both fragments, and the total multiplicities, with the recoil correction applied (outlined and filled squares, respectively). It is notable that $2\nu_{post}$ appears to b essentially independent of TKE.

completely different from the results for lighter projectiles, and initially suggests that the neutrons identified as pre-scission are emitted after the TKE is decided, in other words close to and after scission. The incomplete focusing of neutrons emitted before the fission fragments approach their asymptotic velocity ("acceleration neutrons") causes the multiple-source fit to assign a certain fraction to the pre-scission source. Empirically, it was found [17] that the number of neutrons emitted before the fragments reach 80% of their final velocity is equivalent to the number misidentified as pre-scission in the multiple-source fit. If the lifetime of the composite system before scission is long, the excitation energy is reduced by evaporation, and "acceleration neutrons" will not make a large contribution [19,20,27]. If, however, the lifetime is short, as seems to be the case in these reactions, the converse may be expected [17]. It is possible to argue that the observed TKE dependence could be explained in other ways. For instance, it might be expected that in order to observe a high TKE (compact configuration), the neck must rupture early, while to observe a low TKE (elongated configuration) it must rupture late. The effect of angular momentum could also make a small contribution, since high angular momenta may be associated with shorter lifetimes and with slightly higher TKE values, due to the larger tangential velocity at scission. Also a high velocity at scission may be correlated with both higher TKE and shorter lifetimes. The disagreement between τ_f of $\sim 20\times10^{-21}$ s and the "sticking time" of 6×10^{-21} s, estimated from the rotation angle of the composite system, in conjunction with the poorer quality of the fit to the neutron spectra, indicates that acceleration neutrons must play a major part.

Quantitative calculations have been made, using the computer code JULIAN, of the time dependence of the emission of post-scission neutrons. The parameters used in the calculations were those that resulted in the ν_{tot} values shown in Fig. 20. At scission, it was assumed that the fragments were stationary (thus the time to reach 80% of the final velocity is probably slightly overestimated) and spherical (the neglect of any deformation energy of the fragments during acceleration results in higher excitation energies than will prevail in reality). The actual deformation energy during acceleration will depend in detail on subtle aspects of nuclear viscosity, such as the possible dependence on deformation, and its estimation is beyond the scope of this paper. The two approximations noted above will both result in slightly higher calculated acceleration neutron multiplicities than would prevail in nature. The most important variable determining the neutron lifetimes is a_ν in the fragments, and as in the rest of this work, the expression of Ref. [43] was used, resulting in a_ν between $A/8.35$ and $A/7.95$. For the reaction ^{64}Ni+^{238}U, it was assumed that the reaction time τ_f was 5×10^{-21} s, and the energy shift ΔE_x was 50 MeV, independent of TKE. This resulted in a "true" ν_{pre} value of 1.2. Then, the "acceleration multiplicity," up to 2.5×10^{-21} s after scission was added to this, to represent the apparent ν_{pre} determined in the multiple-source fit to the data. The sum of these multiplicities is given by the concentric circles in Fig. 22. Although not exactly reproducing the data, the agreement is remarkably good, and gives credence to the argued importance of neutron emission during acceleration. The fact that the gradient is not as steep as that of the data could be taken as support for the suggested mechanisms leading to an increase of τ_f as the TKE is reduced. However, the measured TKE dependence of ν_{tot} is substantially different from that calculated, with the measured multiplicity at the lowest TKE values showing a considerable deficit. This may be associated with the large acceleration multiplicity, and simply reflect the fact that the multiple-source-fitting program, which does not account for neutron emission during acceleration, is simply not capable of adequately fitting the measured neutron angular correlation. Also, the locations of the neutron detectors were not optimized to be sensitive to neutrons focused at angles intermediate between the compound system velocity and the asymptotic fragment velocities. These potential problems mean that the measured values of ν_{pre} contain substantial systematic uncertainties, and quantitative conclusions about absolute multiplicities are probably premature. Nevertheless, it is undoubtedly the case that the TKE dependence of the neutron angular correlations is very different

TABLE XV. Neutron multiplicities and statistical model input parameters for the reactions of 417.7 MeV ^{64}Ni.

Target	A(CN)	A(CN)/a_ν	σ_{fus} (mb)	l_{fus}	E_x(CN)[a] (MeV)	ν_{pre} (error)	ε_ν (MeV) (error)	ν_{post} (error)	ν_{tot} (error)	Mass range[b]	TKE[c] (MeV)	σ_{TKE} (MeV)
^{238}U	302	9.15	320	87	75.9	4.00 (0.80)	3.97 (0.22)	5.40 (0.60)	14.80 (0.35)	135–165	266	31.2
^{208}Pb	272	9.05	290	81	81.6	3.25 (0.60)	3.51 (0.21)	4.68 (0.40)	12.60 (0.25)	105–165	237	
^{197}Au	261	9.00	350	88	95.3	3.15 (0.60)	3.86 (0.22)	4.58 (0.40)	12.30 (0.30)	120–140	231	
^{175}Lu	239	8.90	600	113	113.5	3.30 (0.50)	3.98 (0.25)	4.08 (0.25)	11.45 (0.25)	105–130	201	24.6
^{154}Sm	218	8.80	850	118	136.0	3.90 (0.35)	3.97 (0.24)	4.20 (0.25)	12.3 (0.20)	95–123	174	22.0

[a]Excitation energy above the liquid-drop ground state, no pre-equilibrium energy subtracted.
[b]Mass cut applied to the fission fragments for the results tabulated.
[c]TKE for the mass cut applied.

in the ^{64}Ni-induced reactions from all the others measured, and that the data are consistent with a considerable number of neutrons being emitted by the fragments before they reach 80% of their final velocity.

Further improvements in experiments, analysis, and/or reaction simulations should lead to the exciting prospect that absolute neutron widths (lifetimes) may be calibrated against the acceleration time of fission fragments. Preliminary results shown here suggest that calculated lifetimes may be substantially correct, and if confirmed with better precision, will serve to underpin the entire basis upon which fission time scales, and thus nuclear viscosity determinations are made from pre-scission neutron multiplicity measurements.

Accepting the proposition that a fall in ν_{pre} with TKE is an indication that emission during acceleration of the fragments is important, it is clear that the absence of such a gradient in the other reactions is conversely an indiction that it is not a significant contributor to ν_{pre}, and interpretation in terms of τ_f alone is likely to be substantially correct. It should also be the case that the "acceleration multiplicity" contribution to ν_{pre} calculated using JULIAN for other reactions is reasonably accurate, and may be used to correct the value of ν_{pre} obtained from the multiple source fit to the data.

D. Post-scission neutron multiplicity

It is clear that the primary information on the dynamics of the fission process is contained in the pre-scission neutron multiplicity. Additional and supporting information can however be deduced from the post-scission neutron multiplicity.

First, let us consider what physical properties will influence ν_{post}. In the absence of pre-scission emission, the bombarding energy, which determines E_x(CN) of the compound nucleus, would have a large influence. Pre-scission emission is found experimentally to take away most of the extra energy, resulting in only a small increase in ν_{post} with E_x(CN). This means that ν_{post} is sensitive to all the parameters which determine ν_{pre}, being predominantly the pre-scission time τ_f, the energy shift ΔE_x, which reflects the potential energy surface (PES) and the reaction trajectory over it, and the neutron binding energies of the compound nucleus. The latter dependence leads to the paradoxical fact that a neutron deficient system (which will have neutron deficient fission fragments) can give a *larger* value of ν_{post} than a neutron rich system, since ν_{pre} will be smaller in the former case. Of course ν_{post} will be directly influenced by the effective fission Q value (Q_f), the latter dependence is clearly seen in the strong dependence of ν_{post} on TKE and by the binding energies in the fragments. The latter effect can be corrected using statistical model calculations to give the fragment excitation energy.

1. Excitation energy of fission fragments

The post-scission neutrons will carry away the thermal excitation energy at scission plus a certain amount of the deformation energy at scission:

$$E_X^{FF} = E_X^{SCIS} + E_{DEF}^{SCIS} .$$

In order to deduce E_X^{FF} carried by the two fragments, calculations have been carried out (with JULIAN) of the neutron, proton, deuteron, and α particle multiplicities, for excitation energies 15, 30, 50, and 75 MeV, for all fission fragments. The parameters used in the calculations were a level density parameter $a_\nu = A/10$ for $E_X^{FF} > 60$ MeV, while for lower values shell corrections were included. The angular momentum was set to zero. It was further assumed that E_x is divided according to the mass of the fragments, in agreement with experiment (see Figs. 7, 8, 14, 15, 18). Then from the measured ν_{post} values (Tables V, VI, XIII and XV) and those calculated, the mean exci-

TABLE XVI. Mean total excitation energies of both fission fragments (E_x^{FF}) in MeV determined from the measured post-scission neutron multiplicities, for the reactions induced by ^{16}O and ^{18}O. Also tabulated are the effective fission Q value [Q_F(MeV)] and Q_F', an estimate of the average change in excitation energy in MeV between equilibrium and scission (see text), and the fraction (F_{acc}) of fission fragments with neutron emission lifetimes less than the time to reach 80% of the asymptotic velocity (see text).

Projectile	^{18}O					
Target	^{124}Sn	^{144}Sm	^{154}Sm	^{169}Tm	^{197}Au	^{238}U
E_x^{FF}	41	59	49	57	60	88
(error)	(2)	(6)	(2)	(3)	(3)	(4)
Q_F	−37.0	−16.6	−21.6	−6.0	17.2	49.3
Q_F'	−9	−3	−6	6	25	55
F_{acc}	0.20	0.03	0.17	0.17	0.26	0.52
Projectile	^{16}O					
Target	^{109}Ag	^{154}Sm	^{184}W	^{197}Au	^{208}Pb	^{238}U
E_x^{FF}	44	59	74	75	86	109
(error)	(6)	(7)	(5)	(5)	(5)	(7)
Q_F	−39.0	−19.1	2.6	15.4	20.4	47.3
Q_F'	−9	0	17	27	31	55
F_{acc}	0.04	0.06	0.15	0.21	0.34	0.42

tation energy of each fragment was determined; an average over a Gaussian distribution around the symmetric mass $(A_{CN}-\nu_{pre})/2$ with width $\sigma_A/A=\sigma_Z/Z=0.1$ was performed, involving $\gtrsim 100$ isotopes. The total excitation energy carried by both fragments (E_X^{FF}), as determined for each reaction, is shown in Tables XVI and XVII, while Fig. 23 shows E_X^{FF} plotted as a function of the mass number at scission $A(\text{SCIS})=A(\text{CN})-\nu_{pre}$. First we note that most of the ^{16,18}O and ^{40}Ar data points lie in a rather tight band with about 0.33 MeV per nucleon, corresponding to a temperature of 1.6 or 1.8 MeV for $a_\nu=A/8$ or $A/10$, respectively. Since some of this energy will be in the form of deformation energy at the scission configuration, the excitation energy at scission will be lower. The data points for $^{16}O+^{238}U$, for $^{40}Ar+^{238}U$, and for all ^{64}N-induced reactions lie significantly above this band. This can be explained by postulating a shorter pre-scission lifetime for these reactions, resulting in less energy removed by pre-scission emission, and a higher E_X^{FF}. This is in agreement with the trends determined from the pre-scission neutron data.

It may also be instructive to show the variation of E_x^{FF} with the effective fission Q value, which ranges from over 100 MeV for the heaviest system studied, decreasing to -40 MeV for the lightest. This means that the fragments in the latter case have 40 MeV less energy than the compound nucleus, but *only* for zero angular momentum. However, we know that in order to observe measurable yields of fission, the fission barrier height must be reduced to $\lesssim 10$ MeV; thus a large angular momentum must be given to the nucleus, with a correspondingly large rotational energy at the equilibrium deformation. Making use of an approximate expression for the TKE ($\text{TKE}=0.124Z^2/A^{1/3}$), it can be shown that the moment of inertia at scission is 2.45 times larger than for the spherical nucleus (assuming no pre-scission velocity), and thus a fraction 0.6 of the original rotational energy may be translated into thermal energy. Thus it is appropriate to plot E_X^{FF} not against Q_f, but against $Q_f+0.6\bar{E}_{rot}$, where $\bar{E}_{rot}$ is the mean rotational energy of the compound system for those nuclei undergoing fission. Uncertainty in $\bar{E}_{rot}$ due to uncertainty in the mean angular momentum is typically less than ± 5 MeV. Since the system must gain energy from saddle to scission, it follows that the minimum realistic value of $Q_f+0.6\bar{E}_{rot}$ is about -10 MeV, unless extremely low probability events were studied. To further clarify the presentation of the data, both E_X^{FF} and the quantity $Q_f'=(Q_f+0.6\bar{E}_{rot})$ have been divided by A_{SCIS}, and are shown in Fig. 24. Those data points corresponding without doubt to quasifission reactions are filled in. The other points show little or no discernible dependence on Q_f'. If the pre-scission emission were unaffected by Q_f', or in the case of spontaneous fission, where there is no pre-scission emission, there should be a full correlation of E_X^{FF} with Q_f', indicated by the diagonal line. Thus these results for fusion-fission reactions may be taken as indicating that the effect of Q_f' is felt in the pre-scission emission, which is also the conclusion reached from the deduced values of ΔE_x from ε_ν results, at least for $A(\text{CN})>200$. There are of course other possible reasons for this behavior, such as an increase in the fission time scale with A(CN), a strong variation of the level density parameter with A, and neutron emission during fragment acceleration, which would cause the deduced E_X^{FF} values to be too low, and result in ν_{pre} values too high.

2. *Neutron emission during acceleration*

In order to estimate the probability that neutrons are emitted during acceleration of the fragments, the mean evaporation times for the first neutron from all fragments have been calculated, taking $a_\nu=A/10$. It has been shown [17] that neutrons emitted before the fragments reach 80% of their final velocity ($\lesssim 3\times10^{-21}$ s) are misidentified as pre-scission neutrons in the multiple-source fits. For each reaction, the fraction of fission fragments having neutron emission mean lifetimes less than 3×10^{-21} s was calculated, the results being shown in Tables XVI and XVII as F_{acc}. This represents in many respects an upper limit since the velocity at scission is assumed to be zero, the deformation energy of the fragments (unknown) is taken to be zero, and according to the formula of Ref. [43], a level density parameter of

TABLE XVII. As Table XVI, for the ^{40}Ar- and ^{64}Ni-induced reactions.

Projectile	^{40}Ar						
Target	^{141}Pr	^{165}Ho	^{169}Tm	^{181}Ta	^{197}Au	^{208}Pb	^{238}U
$E_x(FF)$	59	78	79	62	76	106	126
(error)	(4)	(11)	(6)	(9)	(7)	(7)	(8)
Q_F	-2.1	13.7	16.3	25.3	42.3	50.0	75.5
Q_F'	15	27	29	35	49	56	80
F_{acc}	0.09	0.24	0.22	0.16	0.23	0.44	0.66
Projectile	^{64}Ni						
Target	^{154}Sm	^{175}Lu	^{197}Au	^{208}Pb	^{238}U		
$E_x(FF)$	134	120	125	114	122		
(error)	(11)	(10)	(15)	(8)	(15)		
Q_F	23.3	48.1	67.7	76.9	106.2		
Q_F'	40	62	75	83	112		
F_{acc}	0.41	0.27	0.39	0.43	0.67		

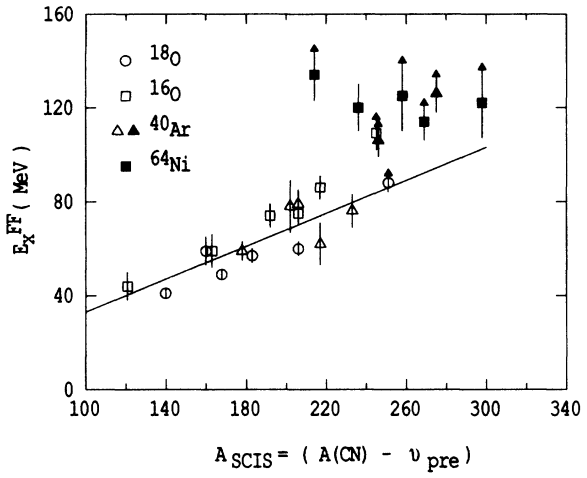

FIG. 23. Deduced excitation energy at scission E_x^{FF} as a function of the mass number at scission. Fusion-fission data points are shown outlined, whilst quasifission points are filled in. Arrowheads at the top of error bars indicate that neutron emission during the acceleration time of the fragments is expected to be important, resulting in a higher E_x^{FF} value than is apparent.

$\sim A/8$ may be more appropriate for most fragments leading to lifetimes twice as short, and thus the values in Tables XVI and XVII may be thought as an upper limit per fragment ($a_\nu = A/10$) or per fission event ($a_\nu = A/8$). Taking an arbitrary limit of ~ 0.4 neutrons emitted during acceleration, in general it is the case that the fusion-fission reactions are below (except for $^{16,18}O+^{238}U$) and the quasifission reactions are above this limit, the points above being indicated in Figs. 23 and 24 by arrowheads on the upper end of the error bars. Thus the effect of neutron emission during acceleration does not substantially affect the fusion-fission results, but for quasifission, will lead to rather higher E_X^{FF} at scission than determined from ν_{post} alone. Using the deduced E_X^{FF} at scission, it should be possible to calculate the lifetime of the last neutron emitted from the compound nucleus before scission. Potential problems arise in estimating appropriate transmission coefficients and binding energies, as in analyzing pre-scission data, and also in thermal excitation energies and level densities, which in the analysis of pre-scission data are to first order fixed by using the measured pre-scission neutron kinetic energy. Using the thermal excitation energy at scission, reduced by the rotational energy of the compound nucleus with angular momentum $60\hbar$, compound nucleus transmission coefficients and binding energies, and $a_\nu = A/10$, results in a lifetime of 25×10^{-21} s averaged over all the fusion-fission reactions, and 2.5×10^{-21} s averaged over the faster reactions. These times are in qualitative agreement with those expected from the discussion of reaction times in earlier sections, and show good consistency between interpretation of pre-scission and post-scission multiplicities. The information lacking in the ν_{post} analysis is the appropriate E_x to use in calculating pre-scission lifetimes, which is in principle carried by the pre-scission neutron energy spectrum.

For bombarding energies higher than those used here, when the initial excitation energy of the compound system may be uncertain, determination of reaction times through ν_{post}, either directly (as here) or through Monte Carlo modeling [25] is more reliable than using ν_{pre}, unless extensive data on competing pre-scission decay channels and on the initial excitation energy are available.

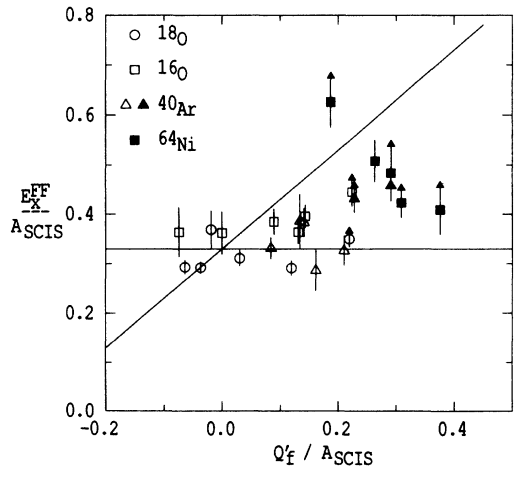

FIG. 24. Deduced excitation energy per nucleon at scission as a function of the effective change in excitation energy during fission (see text), again per nucleon. The horizontal line shows a constant energy per nucleon, while the diagonal line represents the expected trend if the pre-scission emission were completely unaware of the fission Q value. Data points have the same meaning as in Fig. 23.

V. SUMMARY AND CONCLUSION

A new method for interpreting pre-scission neutron data has been presented, based on the use not only of the measured pre-scission neutron multiplicity (ν_{pre}), but also of the mean neutron kinetic energy (ε_ν). Through a statistical model analysis, the latter quantity allows the mean neutron emission rate to be calculated independent of uncertainties in the initial excitation energy of the compound nucleus, the level density parameter, and with less dependence than previously on the trajectory of the nucleus over the potential energy surface as it moves to scission. Thus fission time scales have been determined without many of the systematic uncertainties which plagued previous analyses. Using a model in which fission is totally suppressed for a time τ_f, then attains its full width, the experimental data show that for essentially all fusion-fission reactions, $\tau_f = (35\pm15)\times10^{-21}$ s, apparently with little dependence on the compound nucleus mass (fissility). In this model, the mean neutron kinetic energy ε_ν was reproduced by adjusting the initial compound nucleus excitation energy E_x(CN) (taken to be that of the nucleus at its equilibrium configuration) by adding an energy correction ΔE_x, which represents the average shift in the excitation energy caused by the shape changes occurring in the passage from the most compact configuration (equilibrium or not, depending on the reac-

tion) to scission. It may also compensate for uncertainty in the initial excitation energy and the level density parameter. Simultaneously reproducing ν_{pre} and ε_ν by adjusting both τ_f and ΔE_x for the symmetric fission component of all reactions resulted in the data points shown in Fig. 25, which is a compilation of all the data previously shown. Considering first the τ_f results for fusion-fission (those for measurements where quasifission was observed and acceleration neutrons should contribute significantly are signaled by arrowheads on the error bars), it is very gratifying that for three different experiments, with different kinematic conditions and detector calibrations, the deduced τ_f values are so consistent, showing τ_f is between 20×10^{-21} and 50×10^{-21} s. Some questions still remain to be discussed about the influence of acceleration neutrons for the most neutron-rich heavy nuclei, and the influence of fast fission (fission without barrier); it may be that data with higher statistical accuracy are required to permit definitive conclusions to be drawn from experimental data alone. It must be recalled that the τ_f is not equivalent to the pre-saddle delay time in a model in which the fission width rises gradually to its asymptotic value, since in the case of a low fission barrier and thus high fission width, fission may compete equally with neutron emission well before the full fission width is reached.

The ΔE_x data also show a remarkable clustering, indeed the agreement for heavy nuclei of fusion-fission and quasifission data points is surprising, and points to the need for analysis of the ν_{pre} and ε_ν data by a more sophisticated dynamical/evaporation simulation of fission. The slope of ΔE_x with A(CN) follows the variation of Q_f' quite closely (the latter values are shown by the small outlined diamond-shaped points), however, this may be partly due to the choice of a_ν. It would clearly be useful if the prescription used for a_ν were tested experimentally, so that the interpretation of ΔE_x could proceed with less ambiguity. To illustrate the effect of uncertainty in a_ν, a 10% change in a_ν requires a 10% change in the thermal excitation energy, which must be made by changing ΔE_x; for the heaviest systems this requires a 20% change in ΔE_x, while for lighter nuclei, where ΔE_x is close to zero, the change required is typically 10 MeV. Uncertainty in ΔE_x also results from lack of detailed knowledge of the deposited excitation energy in fusion, and the mean energy tied up in rotation. Independent of these possible problems, it is clear that ε_ν and the neutron energy spectra in general carry very useful information, which should not be neglected.

A strong reduction of ν_{pre} for asymmetric mass splits in heavy-ion-induced fission has been clearly demonstrated for the first time. For fusion fission, this has been explained in terms of phase-space arguments and a reduction in the fission time scale for more asymmetric mass splits; the latter effect has been demonstrated for fission of a system near the Businaro-Gallone point, where the phase-space effects are minimal. A dependence of the dynamical time scale on mass asymmetry will in principle affect the distribution of mass splits observed, favoring asymmetric splits compared to the yields expected on the basis of phase-space arguments alone. This effect should be further investigated, since it seems that it may be quite significant for lighter nuclei. For quasifission, the drop in ν_{pre} seems to be associated principally with the mass-asymmetry dependence of the PES, deduced reaction times being within error independent of asymmetry. This conclusion may be influenced by the importance of neutron emission during acceleration of the fragments for these fast reactions.

In interpreting the TKE dependence of ν_{pre}, recoil

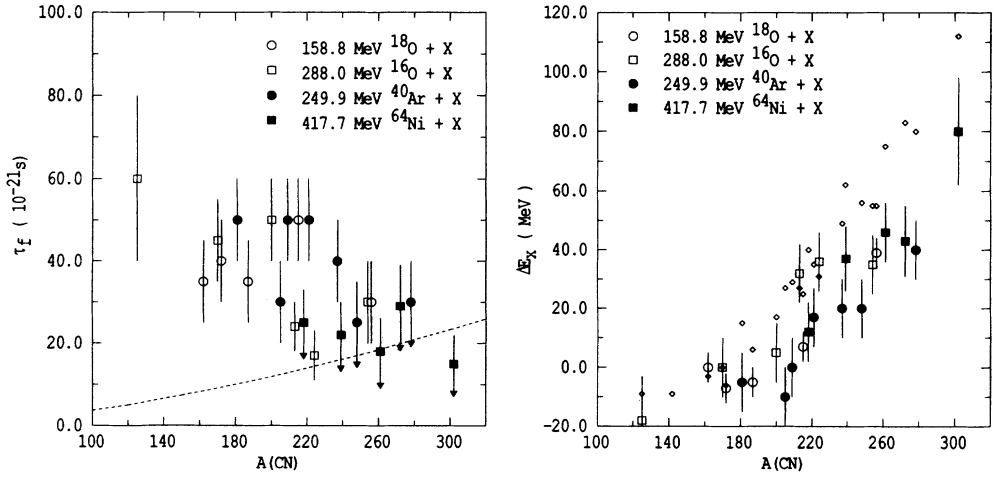

FIG. 25. The left panel shows the deduced values of τ_f for all reactions studied in this work, as a function of the compound nucleus mass number. The time for a complete rotation of a nucleus with the moment of inertia of two touching spheres and angular momentum $70\hbar$ is shown by the dashed line. Downward arrows on the error bars indicate quasifission reactions, where neutron emission during acceleration of the fragments is expected to inflate the deduced τ_f values. The right-hand panel shows the deduced ΔE_x values, together with the values of Q_f' (indicated by the small rhombi). The data follow this trend quite clearly, suggesting that during the pre-scission emission, the effect of fission Q value is clearly felt. The effect on ΔE_x of neutron emission during acceleration is not yet clear.

effects must be taken into account. For fusion-fission reactions, as expected, it was concluded that when all corrections are applied, ν_{pre} is independent of TKE. However, for the ^{64}Ni-induced quasifission reactions, ν_{pre} was found to increase rapidly with decreasing TKE, a trend which the recoil corrections only reinforce. The variation in ν_{pre} accounted for essentially all the increase in energy available due to the lower TKE, since ν_{post} was almost independent of TKE. The first explanation for this effect is neutron emission during acceleration of the fragments, which in the fit appears mainly in the prescission component. Increasing E_x by reducing the TKE results in even shorter lifetimes, and thus an increase in the apparent ν_{pre}. Emission during acceleration would be expected due to the very short lifetime of the composite nuclei ($< 10^{-20}$ s) in the ^{64}Ni-induced reactions. A possible second cause for this experimental observation is that there may be a correlation between the TKE and the lifetime of the composite systems in quasifission reaction, high TKE (compact scission configuration) being correlated with a short lifetime, low TKE with long. This should be further investigated, experimentally and theoretically. The TKE dependence of ν_{pre} may lead to the ability to calibrate neutron emission lifetimes against the fission fragment acceleration time. Present calculations give rather good agreement; however, several simplifying assumptions are used.

Making use of statistical model calculations, the post-scission neutron multiplicities have been converted to the excitation energy at scission. For fusion-fission reactions, this corresponds to an excitation energy per nucleon of approximately 0.33 MeV, independent of the compound nucleus fissility, and increasing only slightly with excitation energy. For quasifission, it is higher. From these results, the lifetime of the last neutron for each reaction has been estimated, yielding times consistent with expectations.

In conclusion, the present series of measurements have revealed a number of new phenomena in heavy-ion induced fission. Their interpretation is not yet quantitatively complete in all cases, but they will help us to understand the complex phenomenon of fission. The use of both ν_{pre} and ε_ν data in the interpretation of neutron measurements in fission clearly represents a significant advance, and in conjunction with the new results obtained as a function of mass split and TKE, should act as a spur to further measurements in this field, not only of neutrons, but also of charged particles, γ rays [53] fission probabilities [54], and mass distributions.

Statistical model calculations with the code JULIAN were performed on the Fujitsu VP100 of the Australian National University Supercomputer Facility. The ^{238}U targets were provided by H. Folger, to whom we are grateful.

[1] A. J. Sierk and J. R. Nix, Phys. Rev. C **31**, 982 (1980).
[2] J. R. Nix and A. J. Sierk, Nucl. Phys. **A428**, 161c (1984).
[3] J. R. Nix, A. J. Sierk, H. Hofmann, F. Scheuter, and D. Vautherin, Nucl. Phys. **A424**, 239 (1984).
[4] S. Grossmann, U. Brosa, and A. Müller, Nucl. Phys. **A481**, 340 (1988).
[5] Ye. N. Gruzintsev, M. G. Itkis, J. V. Kotlov, S. I. Mulgin, V. N. Okolovich, A. Ya. Rusanov, and G. N. Smirenkin, Z. Phys. A **323**, 307 (1986).
[6] Ye. N. Gruzintsev, M. G. Itkis, S. I. Mulgin, V. N. Okolovich, A. Ya. Rusanov, and G. N. Smirenkin, Yad. Fiz. **43**, 1101 (1986) [Sov. J. Nucl. Phys. **43**, 703 (1986)].
[7] J. Tōke, R. Bock, G. X. Dai, A. Gobbi, S. Gralla, K.D. Hildenbrand, J. Kuzminski, W. J. F. Müller, A. Olmi, H. Stelzer, B. B. Back, and S. Bjørnholm, Nucl. Phys. **A440**, 327 (1985); W. Q. Shen, J. Albinski, A. Gobbi, S. Gralla, K. D. Hildenbrand, N. Hermann, J. Kuzminski, W. F. J. Müller, H. Stelzer, J. Tōke, B. B. Back, S. Bjørnholm, and S. P. Sørensen. Phys. Rev. C **36**, 115 (1987).
[8] P. Gippner, K. D. Schilling, W. Seidel, F. Stary, E. Will, H. Sodan, S. M. Lukyanov, V. S. Salamatin, Yu. E. Penionzhkevich, G.G. Chubarian, and R. Schmidt, Z. Phys. A **325**, 335 (1986).
[9] H. Feldmeier, in *Proceedings of Tsukuba International Symposium, 1984,* edited by K. Furuno and T. Kishimoto (World Scientific, Singapore, 1985).
[10] B. B. Back, Phys. Rev. C **31**, 2104 (1985).
[11] H. Rossner, J. R. Huizenga, and W. U. Schröder, Phys. Rev. C **33**, 560 (1986).
[12] R. Freifelder, P. Braun-Munzinger, P. DeYoung, R. Schicker, S. Sen, and J. Stachel, Phys. Rev. C **35**, 2097 (1987).
[13] K. Lützenkirchen, J. V. Kratz, G. Wirth, W. Brüchle, K. Sümmerer, R. Lucas, J. Poitou, and C. Grégoire, Nucl. Phys. **A452**, 351 (1986).
[14] D. Hilscher, E. Holub, U. Jahnke, H. Orf, and H. Rossner, in *Proceedings of the Third Adriatic Europhysics Study Conference, Hvar, Yugoslavia, 1981,* edited by N. Cindro, R. A. Ricci, and W. Greiner (North-Holland, Amsterdam, 1981), p. 225; E. Holub, D. Hilscher, G. Ingold, U. Jahnke, H. Orf, and H. Rossner, Phys. Rev. C **28**, 252 (1983).
[15] A. Gavron, J. R. Beene, B. Cheynis, R. L. Ferguson, F. E. Obenshain, F. Plasil, G. R. Young, G. A. Petitt, R. Jääskeläinen, D. G. Sarantites, and C. F. Maguire, Phys. Rev. Lett. **47**, 1255 (1981); **48**, 835(E) (1982).
[16] D. Ward, R. J. Charity, D. J. Hinde, J. R. Leigh, and J. O. Newton, Nucl. Phys. **A424**, 189 (1983).
[17] D. J. Hinde, R. J. Charity, G. S. Foote, J. R. Leigh, J. O. Newton, S. Ogaza, and A. Chatterjee, Phys. Rev. Lett. **52**, 986 (1984); **53**, 2275(E) (1984).
[18] W. P. Zank, D. Hilscher, G. Ingold, U. Jahnke, M. Lehmann, and H. Rossner, Phys. Rev. C **33**, 519 (1986).
[19] D. J. Hinde, R. J. Charity, G. S. Foote, J. R. Leigh, J. O. Newton, S. Ogaza, and A. Chatterjee, Nucl. Phys. **A452**, 550 (1986).
[20] A. Gavron, A. Gayer, J. Boissevain, H. C. Britt, T. C. Awes, J. R. Beene, B. Cheynis, D. Drain, R. L. Ferguson, F. E. Obenshain, F. Plasil, G. R. Young, G. A. Petitt, and C. Butler, Phys. Rev. C **35**, 579 (1987).

[21] D. J. Hinde, J. R. Leigh, J. J. M. Bokhorst, J. O. Newton, R. L. Walsh, and J. E. Boldeman, Nucl. Phys. **A472**, 318 (1987).
[22] J. O. Newton, D. J. Hinde, R. J. Charity, J. R. Leigh, J. J. M. Bokhorst, A. Chatterjee, G. S. Foote, and S. Ogaza, Nucl. Phys. **A483**, 126 (1988).
[23] D. J. Hinde, H. Ogata, M. Tanaka, T. Shimoda, N. Takahashi, A. Shinohara, S. Wakamatsu, K. Katori, and H. Okamura, Phys. Rev. C **37**, 2923 (1988).
[24] D. J. Hinde, H. Ogata, M. Tanaka, T. Shimoda, N. Takahashi, A. Shinohara, S. Wakamatsu, K. Katori, and H. Okamura, Phys. Rev. C **39**, 2268 (1989).
[25] D. Hilscher, H. Rossner, B. Cramer, B. Gebauer, U. Jahnke, M. Lehmann, E. Schwinn, M. Wilpert, Th. Wilpert, H. Frobreen, E. Mordhorst, and W. Scobel, Phys. Rev. Lett. **62**, 1099 (1989).
[26] D. J. Hinde, D. Hilscher, and H. Rossner, Nucl. Phys. **A502**, 497c (1989).
[27] H. Rossner, D. Hilscher, D. J. Hinde, B. Gebauer, M. Lehmann, M. Wilpert, and E. Mordhorst, Phys. Rev. C **40**, 2629 (1989).
[28] E. Mordhorst, M. Strecker, H. Frobeen, M. Gasthuber, W. Scobel, B. Gebauer, D. Hilscher, M. Lehmann, H. Rossner, and Th. Wilpert, Phys. Rev. C **43**, 716 (1991).
[29] H. Rossner, D. Hilscher, and D. J. Hinde, Phys. Rev. C **43**, 2434 (1991).
[30] G.F. Peaslee, N. N. Ajitanand, J. M. Alexander, D. Guerreau, R. Lacey, L. C. Vaz, M. Kaplan, M. Kildir, D. J. Moses, D. Logan, and M. S. Zisman, Phys. Rev. C **38**, 1730 (1988) and references therein.
[31] L. Schad, H. Ho, G.-Y. Fan, B. Lindl, A. Pfoh, R. Wolski, and J. P. Wurm, Z. Phys. **A318**, 179 (1984).
[32] B. Lindl, A. Brucker, M. Bantel, H. Ho, R. Muffler, L. Schad, M. G. Trauth, and J. P. Wurm, Z. Phys. A **328**, 85 (1987).
[33] H. Ikezoe, N. Shikazono, Y. Nagame, Y. Sugiyama, Y. Tomita, K. Ideno, A. Iwamoto, and T. Ohtsuki, Phys. Rev. C **42**, 342 (1990).
[34] J. P. Lestone, J. R. Leigh, J. O. Newton, D. J. Hinde, J. X. Wei, Y. Chen, S. Elfström, and D. G. Popescu, Phys. Rev. Lett. **67**, 1078 (1991).
[35] K. H. Bhatt, P. Grangé, and B. Hiller, Phys. Rev. C **33**, 954 (1986) and references therein.
[36] B. Gebauer and Th. Wilpert, Hahn-Meitner-Institut Berlin Annual Report 1984, p. 94; B. Gebauer, M. Wilpert, and Th. Wilpert, Hahn-Meitner-Institut Berlin Annual Report 1986, p. 86; B. Gebauer, M. Wilpert, and Th. Wilpert, Hahn-Meitner-Institut Berlin Annual Report 1987, p. 78.
[37] R. A. Cecil, B. D. Anderson, and R. Madey, Nucl. Instrum. Methods **161**, 439 (1979).
[38] V.E. Viola, K. Kwiatkowski, and M. Walker, Phys. Rev. C **31**, 1550 (1985).
[39] R. J. Charity, J. R. Leigh, J. J. M. Bokhorst, A. Chatterjee, G. S. Foote, D. J. Hinde, J. O. Newton, S. Ogaza, and D. Ward, Nucl. Phys. **A457**, 441 (1986).
[40] R. Bass, Phys. Rev. Lett. **39**, 265 (1977).
[41] A. Gavron, J. Boissevain, H. C. Britt, K. Eskola, M. M. Fowler, H. Ohm, J. B. Wilhelmy, T. C. Awes, R. L. Ferguson, F. E. Obenshain, F. Plasil, G. R. Young, and S. Wald, Phys. Rev. C **30**, 1550 (1984); L. C. Vaz, D. Logan, E. Duek, J. M. Alexander, M. F. Rivet, M. S. Zisman, M. Kaplan, and J. W. Ball, Z. Phys. **A315**, 169 (1984).
[42] M. Blann (private communication).
[43] J. Tōke and W. J. Swiatecki, Nucl. Phys. **A372**, 141 (1981).
[44] U. L. Businaro and S. Gallone, Nuovo Cim. **1**, 629 (1955).
[45] L. G. Sobotka, M. A. McMahan, R. J. McDonald, C. Signarbieux, G. J. Wozniak, M. L. Padgett, J. H. Gu, Z. H. Liu, Z. Q. Yao, and L. G. Moretto, Phys. Lett. **53**, 2004 (1984).
[46] E. Plagnol, L. Vinet, D. R. Bowman, Y. D. Chan, R. J. Charity, E. Chavez, S. B. Gazes, H. Han, W. L. Kehoe, M. A. McMahan, L. G. Moretto, R. J. Stokstad, G. J. Wozniak, and G. Auger, Phys. Lett. B **221**, 11 (1989).
[47] H. Y. Han, K. X. Jing, E. Plangnol, D. R. Bowman, R. J. Charity, L. Vinet, G. J. Wozniak, and L. G. Moretto, Nucl. Phys. **A492**, 138 (1989); L.G. Moretto and G. J. Wozniak, Pramana - J. Phys. **33**, 209 (1989).
[48] U. Lynen, J. Pochodzalla, W. Trautmann, N. Brummund, E. Eckert, R. Glasow, K. D. Hildenbrand, L. H. Kamperd, W. F. J. Müller, D. Pelte, H. J. Rabe, H. Sann, R. Santo, H. Stelzer, and R. Wada, Phys. Rev. Lett. **59**, 2844 (1987); J. Pochodzalla, R. J. Charity, U. Lynen, H. Sann, W. Trautmann, and R. Trockel, Phys. Rev. C **40**, 2918 (1989).
[49] H. C. Britt, B. H. Erkkila, R. H. Stokes, H. H. Gutbrod, F. Plasil, R. L. Ferguson, and. M. Blann, Phys. Rev. C **13**, 1483 (1976); R. Lacey, N. N. Ajitanand, J. M. Alexander, D. M. de Castro Rizzo, G. F. Peaslee, L. C. Vaz, M. Kaplan, M. Kildir, G. LaRana, D. J. Moses, W. E. Parker, D. Logan, M. S. Zisman, P. DeYoung, and L. Kowalski, *ibid.* **37**, 2540 (1988); B. Borderie, M. Berlanger, D. Gardès, F. Hanappe, L. Nowicki, S. Argarwal, J. Girard, C. Grégoire, J. Matuszeck, and C. Ngô, Z.Phys. A **299**, 263 (1981); H.-G. Clerc, J. G. Keller, C.-C. Sahm, K.-H. Schmidt, H. Schulte, and D. Vermeulen, Nucl. Phys. **A419**, 571 (1984); J. Péter, C. Ngô, F. Plasil, B. Tamain, M. Berlanger, and F. Hanappe, Nucl. Phys. **A279**, 110 (1977); S. Agarwal, J. Galin, B. Gatty, D. Guerreau, M. Lefort, X. Tarrago, R. Babinet, J. Girard, and H. Nifenecker, Z. Phys. **A283**, 173 (1977); C. Ngô, J. Péter, B. Tamain, M. Berlanger, and F. Hanappe, Z. Phys. A **283**, 161 (1977); D. Logan, H. Delagrange, M. F. Rivet, M. Rajagopalan, J. M. Alexander, M. Kaplan, M. S. Zisman, and E. Duek, Phys. Rev. C **22**, 1080 (1980); Z. Zheng, B. Borderie, D. Gardes, H. Gauvin, F. Hanappe, J. Péter, M. F. Rivet, B. Tamain, and A. Zaric, Nucl. Phys. **A422**, 447 (1984).
[50] K. T. Lesko, W. Henning, K. E. Rehm, G. Rosner, J. P. Schiffer, G. S. F. Stephans, B. Zeidman, and W. S. Freeman, Phys. Rev. C **34**, 2155 (1986).
[51] R. Bock, Y. T. Chu, M. Dakowski, A. Gobbi, E. Grosse, A. Olmi, H. Sann, D. Schwalm, U. Lynen, W. Müller, S. Bjørnholm, H. Esbensen, W. Wölfli, and E. Morenzoni, Nucl. Phys. **A388**, 334 (1982).
[52] R. J. Charity (private communication).
[53] M. Thoennessen, D. R. Chakrabarty, M. G. Herman, R. Butsch, and P. Paul, Phys. Rev. Lett. **59**, 2860 (1987).
[54] E.-M. Eckert, A. Kühmichel, J. Pochodzalla, K. D. Hildenbrand, U. Lynen, W. F. J. Müller, H. J. Rabe, H. Sann, H. Stelzer, W. Trautmann, R. Trockel, R. Wada, C. Cerruti, P. Lhénoret, R. Lucas, C. Mazur, C. Ngô, M. Ribrag, E. Tomasi, A. Demeyer, and D. Guinet, Phys. Rev. Lett. **64**, 2483 (1990).